Form Approved
OMB No. 0704-0188

1. AGENCY USE ONLY (Leave blank)	2. REPORT DATE	3. REPORT TYPE AND DATES COVERED
	1 February 1994	Final Technical Report Jul91-Nov93

4. TITLE AND SUBTITLE
Unsteady Flow Field of Large-Amplitude Pitching Airfoils

5. FUNDING NUMBERS
PE - 61102 F
PR - 2307
TA - A3
G - AFOSR-89-0417

6. AUTHOR(S)
M. M. Koochesfahani

7. PERFORMING ORGANIZATION NAME(S) AND ADDRESS(ES)
Michigan State University
East Lansing, MI 48824

8. PERFORMING ORGANIZATION REPORT NUMBER
AFOSR-TR- 94 0355

9. SPONSORING / MONITORING AGENCY NAME(S) AND ADDRESS(ES)
AFOSR/NA
110 Duncan Avenue, Suite B115
Bolling AFB, DC 20332-0001

NA

10. SPONSORING / MONITORING AGENCY REPORT NUMBER
AFOSR-89-0417

11. SUPPLEMENTARY NOTES

12a. DISTRIBUTION / AVAILABILITY STATEMENT
Approved for public release; distribution is unlimited

12b. DISTRIBUTION CODE

13. ABSTRACT *(Maximum 200 words)*

This research program investigated the physical mechanisms involved in the onset of leading edge separation when airfoils pitch to high angles of attack. Both constant pitch rate and variable pitch rate motions were considered. The highlights of results from a combined experimental and computational effort are described in this report. The conclusions from this research indicate the need for boundary-layer resolved measurements of the flow behavior near the leading edge and the evolution of the reverse flow regions on the suction surface. Furthermore, the deliberate shaping of the pitch trajectory for the purpose of optimization of separation delay is suggested as one way to manage the flow and aerodynamic behavior of an airfoil.

14. SUBJECT TERMS	15. NUMBER OF PAGES
Dynamic Stall, Unsteady Separation	32
	16. PRICE CODE

17. SECURITY CLASSIFICATION OF REPORT	18. SECURITY CLASSIFICATION OF THIS PAGE	19. SECURITY CLASSIFICATION OF ABSTRACT	20. LIMITATION OF ABSTRACT
Unclassified	Unclassified	Unclassified	UL

Unsteady Flow Field of Large-Amplitude Pitching Airfoils

Manoochehr M. Koochesfahani†

Department of Mechanical Engineering
Michigan State University
East Lansing, Michigan 48824

Air Force Office of Scientific Research
Grant No. AFOSR-89-0417
Final Technical Report

1-February-1994

† Associate Professor; Principal Investigator.

1. Introduction

The general goal of this research program was to study the various physical mechanisms involved in the onset of leading-edge separation and vortex formation when airfoils execute highly unsteady motions. Unsteady separation and dynamic stall are inherently complex processes which are influenced by many interrelated flow parameters. Instead of a parametric study, our investigation attempted to isolate the basic fluid mechanical phenomena for the specific case of incompressible flow around a NACA-0012 airfoil pitching (about the 1/4-chord axis) to large angles of attack (typically 60 degrees). Both constant pitch rate (i.e. ramp-type) motions, and variable pitch rate motions were studied.

Our work initially started as purely an experimental investigation and quickly lead to a coordinated experimental and computational effort. The computational work - a collaboration with Dr. Miguel Visbal (WPAFB) - allowed us to obtain information on the flow variables that were difficult to measure (such as vorticity and reversed flow evolution near the surface) for our experiments. This close collaboration between experiment and computation has proved to be an ideal approach in the study of such complicated phenomena as leading edge separation and dynamic stall.

This final report provides a brief summary of the highlights of our results to date. Most of these results have been described in much greater detail in previous annual reports [1-4] and conference presentations/papers [5-7]. Some of the results have recently appeared in a journal publication (see Appendix A); one paper is currently under review (see Appendix B). Two other manuscripts are being prepared for publication. This report will conclude by discussing some of the outstanding issues which need further research.

1. Summary of Results for Constant Pitch Rate

The experiments and computations for this case involved very rapid acceleration to a constant pitch rate trajectory. The chord Reynolds number was of order 10^4 ($8{,}000 \leq Re_c \leq 15{,}000$) and non-dimensional pitch rate varied between $0.015 \leq \Omega^* \leq 0.4$. The main findings were:

- The onset of leading edge separation can be determined from flow visualization experiments by marking the appearance of a kink or a "bulge" near the leading edge. Computations show that this feature correlates very well with the appearance of a similar feature in the vorticity field. Visual and numerical predictors of the

separation angle, determined from the computations, agree well with our experimental results.

- The shear layer that forms between the region of reversed flow near the airfoil surface and the outer inviscid stream appears to behave like a "free" shear layer. It is subject to Kelvin-Helmholtz instability and exhibits many of the vortex interactions (such as pairing) observed in free shear layers. Since a counter flow situation exists, this shear layer may exhibit absolute (as opposed to convective) instability characteristics under some conditions.

- At low pitch rates, onset of leading edge separation occurs after the reverse flow originating from the trailing edge has reached the leading edge (see Figure 1).

- At high pitch rates, flow separation is leading-edge dominated; a region of reverse flow develops near the leading edge independently from that originating from the trailing edge (see Figure 2).

- Various estimators for determining the onset of leading edge separation were compared. These estimators were based on the behavior of the vorticity field, the reverse-flow evolution near the surface, surface pressure and pressure gradient fields. All estimators showed the same trend for separation angle versus non-dimensional pitch rate. The estimator based on the evolution of reverse-flow appears to hold the best promise for flow control applications.

2. Summary of Results for Non-Constant Pitch Rate

Studies of non-constant pitch rate included two types of motions. First were airfoil trajectories which deviated from the ideal ramp due to finite acceleration and deceleration periods. Second were variable pitch trajectories constructed from three constant pitch rate segments with non-dimensional pitch rates of $0.5\Omega^*$, Ω^*, and $2\Omega^*$.

(a) Effect of Initial Acceleration

- The elapsed time for onset of leading edge separation is affected by the initial acceleration.

- The angle of attack where separation is observed is <u>not</u> sensitive to initial acceleration for the relatively high pitch rate motions studied.

- Many of the details of dynamic stall vortex formation and its interactions (e.g. convection speed U_c) appear to be also unaffected by the initial acceleration.

- The initial acceleration was observed to affect the integrated loads, surface pressure distribution, and the evolution of the reverse flow regions only during the acceleration period and for a relatively short time ($\tau \equiv tU_\infty/C \leq 0.25$) afterwards. After that time, all of these quantities depend only on the instantaneous angle of attack for a given pitch rate.

(b) Variable Pitch Rate Results

- The instantaneous pitch rate $\dot{\alpha}_{s.s.}$ at the static stall angle, believed to be important for the case of oscillating airfoils, was found not to be a controlling parameter in general.

- Our working hypothesis implies that if the airfoil motion time scale is fast, onset of leading edge separation is expected to be based on the current pitch rate (and angle of attack), and not the details of the motion history up to that point in time. Using this idea, the knowledge of the variation of separation angle α_{sep} versus pitch rate Ω^* for constant pitch rate motions is sufficient to construct a model to predict the separation angle for the three-segment trajectory experiments. The model performs remarkably well for high pitch rates; the agreement with the experiments is somewhat less satisfactory at lower range of pitch rates.

- Shaping the pitch trajectory can be used to delay the onset of leading edge separation beyond that achieved with constant pitch rate motions.

3. Conclusions

The basic physical understanding of the mechanisms for 2-D incipient leading-edge separation is still not complete. This is true even for relatively low Reynolds numbers of order 10^4 where computational results are available. Due to lack of appropriate experimental results, the adequacy of these computations is hard to assess. Most needed are the details of the flow behavior (e.g. the velocity field) within the boundary layer near the leading edge and the evolution of the reverse-flow regions. Such boundary-layer resolved measurements are outside the reach of traditional measurement techniques. Novel diagnostics based on molecular tagging techniques offer new possibilities for these types of measurements covering chord Reynolds numbers from 10^4 to 10^6.

Another issue that requires more attention is the flow behavior for variable pitch rate trajectories. The majority of studies to date have concentrated on either sinusoidal or constant pitch rate motions. Our preliminary results indicate that the onset of leading edge separation can be delayed further when variable pitch rate motions are considered. The deliberate shaping of the pitch trajectory for the purpose of optimization of separation delay is one way to manage the flow and aerodynamic behavior of an airfoil.

4. References

1. Koochesfahani, M. M., Brown, T. A. and Chakrabarti, S. [1990] "Unsteady flow field of large-amplitude pitching airfoils," Annual Progress Report, AFOSR Grant No. AFOSR-89-0417, 31-Dec-1990.

2. Koochesfahani, M. M. and Gendrich, C. P. [1992] "Unsteady flow field of large-amplitude pitching airfoils," Annual Progress Report, AFOSR Grant No. AFOSR-89-0417, 9-March-1992.

3. Koochesfahani, M. M. [1993] "Unsteady flow field of large-amplitude pitching airfoils," Annual Progress Report, AFOSR Grant No. AFOSR-89-0417, 12-February-1993.

4. Koochesfahani, M. M., Smiljanovski, V and Brown, T. A. [1990] "Effect of initial acceleration on the development of the flow field of an airfoil pitching at constant rate." *Proceedings of the NASA/AFOSR/ARO Workshop on Physics of Forced Unsteady Separation*, April 17-19, 1990, NASA Ames Research Center; NASA Conference Publication 3144, 1992, 317-332.

5. Brown, T. A. [1992] "Effects of motion history on leading edge separation for an airfoil pitching to large angles of attack." M. S. thesis, Michigan State University

6. Gendrich, C. P., Koochesfahani, M. M. and Visbal, M. R. [1992] "The visual and vortical signature of leading edge separation." *Bull. Am. Phys. Soc.*, **37(8)**, 1747.

7. Gendrich, C. P., Koochesfahani, M. M. and Visbal, M. R. [1993] "Initial acceleration effects on the flow field development around rapidly pitching airfoils." AIAA-93-0438.

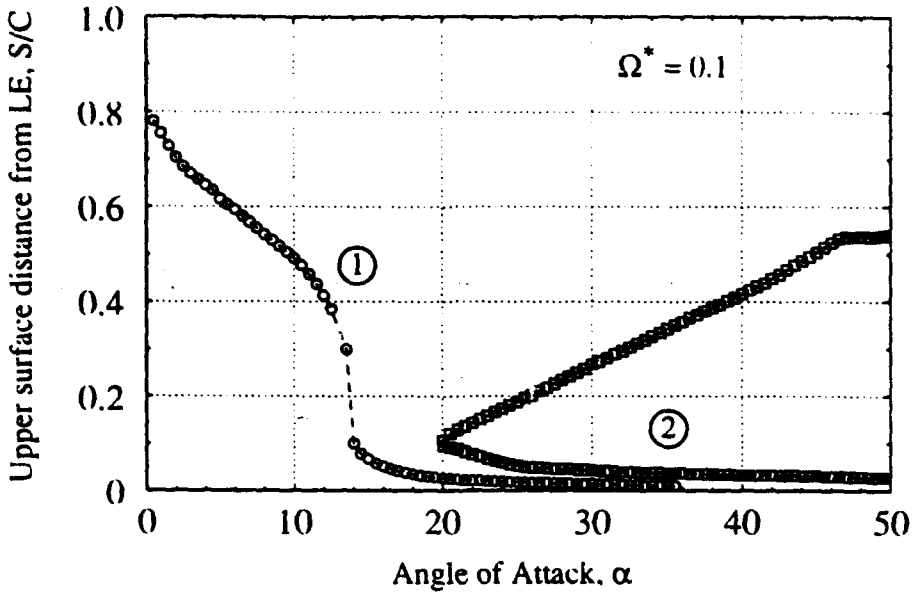

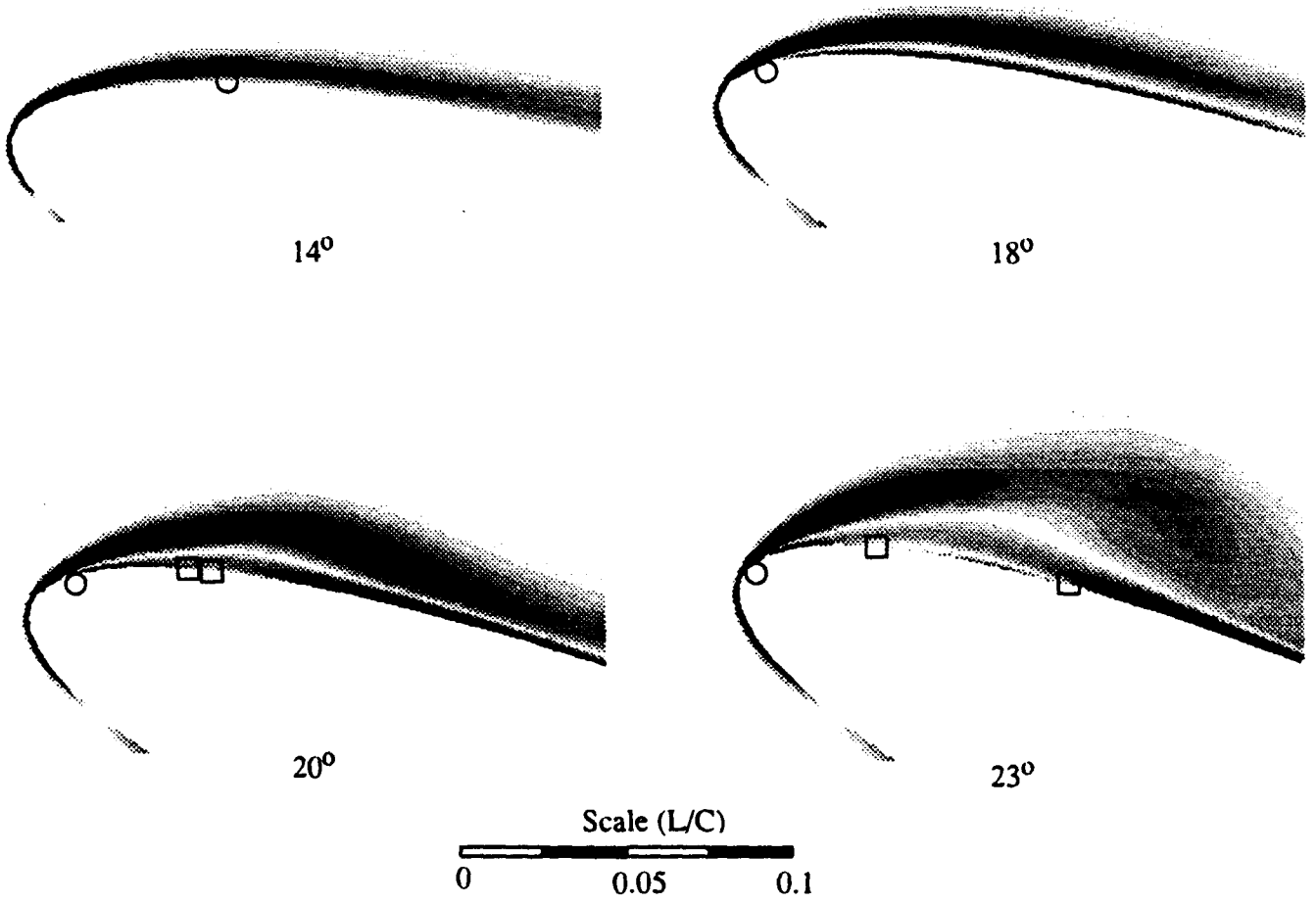

Figure 1. Tangential velocity flow reversal locations just above the airfoil surface and the vorticity magnitude contours at selected angles of attack ($\Omega^* = 0.1$). Curve labeled (1) and the circle symbol indicate the reverse flow front originating at the trailing edge. Curve labeled (2) and the square symbol indicate a new region of forward flow.

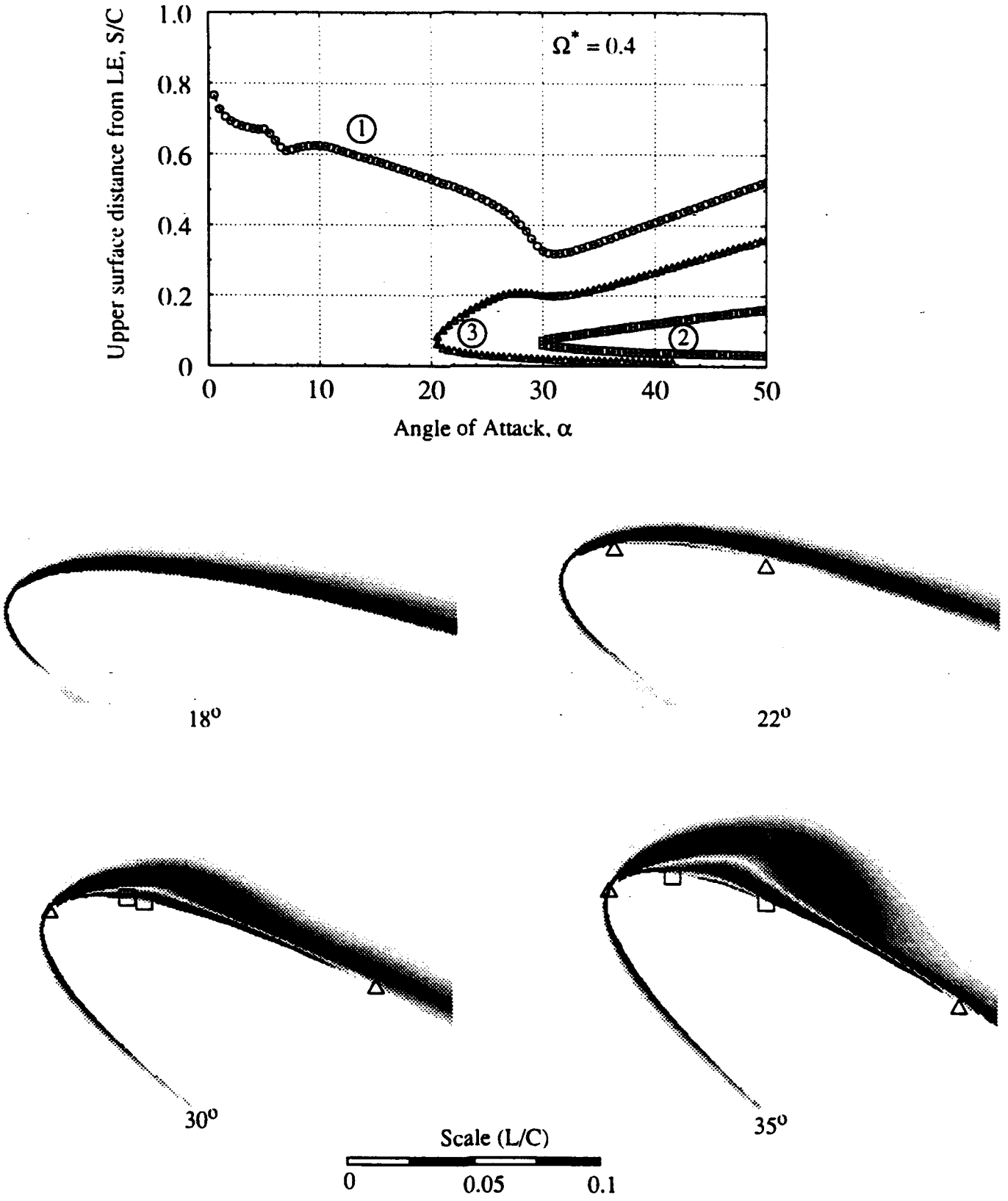

Figure 2. Tangential velocity flow reversal locations just above the airfoil surface and the vorticity magnitude contours at selected angles of attack ($\Omega^* = 0.4$). Curve labeled (1) and the circle symbol indicate the reverse flow front originating at the trailing edge. Curve labeled (3) and the triangle symbol indicate the appearance of a new independent reverse flow region. Curve (2) and the square symbol indicate the region of forward flow.

APPENDIX A

AIAA Journal, Vol. 31, No. 8, 1993

lent Reacting Multi-Phase Flows," *4th International Symposium on Transport Phenomena in Heat and Mass Transfer* (Sydney, Australia), Vol. 1, 1991, pp. 391-401.

[13]Chan, S. H., and Tan, C. C., "Complex Equilibrium Calculation by Simplex and Duality Theories with Applications to Liquid Metal Fuel Propulsion Systems," *Combustion and Flame*, Vol. 88, Feb. 1992, pp. 123-136.

[14]Parnell, L. A., Gilchrist, J. T., and Rogerson, D. J., "Flash and Real-Time Radiographic Study of Closed Liquid Metal Combustion," *2nd Office of Naval Research Propulsion Meeting* (Irvine, CA), Oct. 1989, pp. 188-205.

Initial Acceleration Effects on Flow Evolution Around Airfoils Pitching to High Angles of Attack

Manoochehr M. Koochesfahani* and
Vanco Smiljanovski†
Michigan State University,
East Lansing, Michigan 48824

Introduction

AIRFOILS pitching rapidly to high angles of attack, and the accompanying phenomenon of dynamic stall, were first investigated for the case of sinusoidal motions. The progress in this area is reviewed by McCroskey[1] and Carr.[2] More recently, constant pitch rate (i.e., ramp) motions have been receiving a great deal of attention due to their applicability to supermaneuverable aircraft. Some of the earlier measurements of integrated load[3-5] have now been complemented by computational results[6,7] and high-resolution surface pressure measurements[8]; whole-field velocity information is also becoming available.[9]

Investigations into airfoils pitching at constant rate have typically considered airfoils pitching from a zero angle of attack to some large angle α_{max} well beyond the static stall angle. It has been established that a major parameter governing the flow behavior is the nondimensional pitch rate $\Omega^* = \dot{\alpha}C/(2U_\infty)$, where $\dot{\alpha}$ is the constant pitch rate, C the chord, and U_∞ the freestream speed. It is clear that, in reality, the actual motion of the airfoil must deviate from the ideal ramp due to the finite acceleration and deceleration periods imposed by the damping of the drive system and the response characteristics of the airfoil. The computations of "nominally" constant pitch rate motions also include a brief initial acceleration period. To our knowledge, a systematic investigation of the effects of initial acceleration on the flow characteristics of an airfoil pitching to high angles of attack has not been undertaken. We note that studying such effects can provide not only further insight into the processes of vorticity generation and accumulation on unsteady surfaces, but also clues as to how these processes may be modified or controlled by the deliberate shaping of the pitch-motion trajectory.

In the present experiments, flow visualization is used to monitor the onset of leading-edge separation and the subsequent dynamic stall vortex development as the initial acceleration is systematically varied in magnitude and duration through the acceleration phase to constant pitch rate. The work presented here considers the case of incompressible flow at low-chord Reynolds numbers and relatively high pitch rate.

Received Oct. 13, 1992; revision received Feb. 10, 1993; accepted for publication Feb. 10, 1993.

*Associate Professor, Department of Mechanical Engineering. Member AIAA.

†Graduate Assistant, Exchange Student, Rheinisch Westfälische Technische Hochschule, Aachen, Germany.

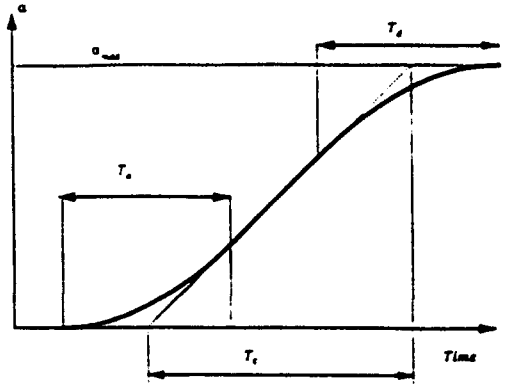

a) Definition sketch; $e = T_a/T_c$

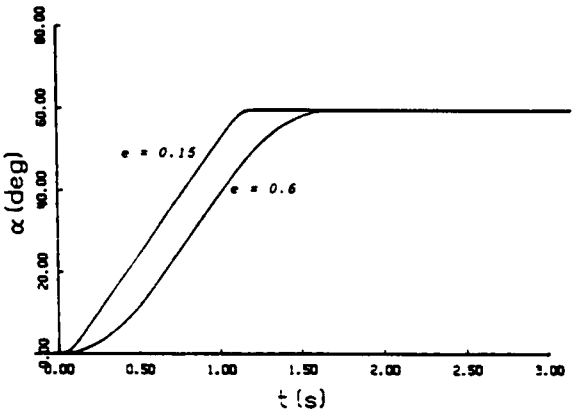

b) Example of actual trajectory executed by the airfoil: $\Omega^* = 0.4$

Fig. 1 Constant pitch rate motion with finite acceleration and deceleration.

Experimental Setup

The experiments were performed in a water channel (Engineering Laboratory Design, Inc.) with a test section 60 × 60 cm in cross section and 240 cm in length. The airfoil was an NACA 0012 with a uniform chord of $C = 8$ cm, a span of $b = 45$ cm, and was fitted on both ends with false walls parallel to the water channel walls. For the results described here, the freestream seed was set to $U_\infty = 10$ cm/s resulting in a chord Reynolds number of 8×10^3. A dc servo motor and a digitial servo controller (Galil, DMC-610) were used to pitch the airfoil about the quarter chord. The pitch-motion trajectory started at zero angle of attack, reached the desired constant pitch rate of $\dot{\alpha}$ after a period T_a of constant acceleration, and stopped at the final angle of attack of 60 deg after a period T_d of constant deceleration (see Fig. 1a). The acceleration and deceleration periods were kept equal in this work. We characterize the pitch trajectory by the nondimensional pitch rate Ω^* and an acceleration parameter $e = T_a/T_c$, where T_c is the "ideal" constant pitch rate time scale needed for the motion. Note that the parameter e gives an indication of the fraction of the motion time used for acceleration/deceleration. The particular cases considered in this study correspond to ($\Omega^* = 0.4$; $e = 0.6$, 0.15, 0.037) and ($\Omega^* = 0.2$; $e = 0.15$, 0.037). Typical examples of the actual pitch trajectory executed by the airfoil are shown in Fig. 1b.

The evolution of the flow was monitored using the hydrogen-bubble technique and laser sheet illumination at the airfoil midspan location. The hydrogen-bubble wire was placed approximately 1 mm upstream of the airfoil leading edge and was pulsed at 20 Hz. Flow images were sensed by a charge coupled device camera at a rate of 60 fields/s with an exposure time of 2 ms/field and acquired by a digital image acquisition system (Recognition Concepts, Inc., TRAPIX-5500) onto a hard disk in real time.

Results and Discussion

The evolution of the flowfield for the case ($\Omega^* = 0.4$; $e = 0.15$) is illustrated in Fig. 2. For each picture, the instantaneous angle of attack and the elapsed time from the start of the motion are indicated. The flow follows the contour of the airfoil, and in that sense appears fully attached, up to an angle of attack $\alpha = 27$ deg. By the time the airfoil has reached $\alpha = 34$ deg, leading-edge separation and vortex formation have already begun with a visual signature of a perturbation near the leading edge. The first visual indication of onset of leading-edge separation and vortex formation was found to occur at ($T_s = 0.64$ s; $\alpha_s = 32$ deg) after close inspection of the image time sequence; T_s and α_s refer to the elapsed time and angle of attack at the onset of leading-edge separation. It should be noted that, based on the image acquisition rate, we estimate the value of α_s to ± 1 deg accuracy. The sequence of pictures in Fig. 2 also shows how the leading-edge vortex grows in time and evolves into the dynamic stall vortex. The flow evolution shown in this figure, including the formation of multiple large-scale vortices above the suction surface, is similar to the known computational and experimental results.

The effect of initial acceleration period on the onset of leading-edge separation for the cases considered here were determined from data similar to Fig. 2. The results are summarized in Table 1.

The results show that the onset of leading-edge separation is delayed to a larger angle of attack as the pitch rate increases. This is consistent with the well-established dynamic stall delay for increasing pitch rate.[1-9] The most important observation, however, is that while the elasped time for leading-edge separation and vortex formation is affected by initial acceleration, the angle of attack where this occurs remains virtually unchanged. In fact, many of the details of subsequent flow development are also nearly the same. Figure 3 shows a comparison at selected angles of attack for two cases with $\Omega^* = 0.4$ and initial accelerations which are different by a factor of 4. Note the similarity of the various events at similar angles of attack; there is, of course, a time shift between the occurrence of similar events in the two cases, as indicated earlier.

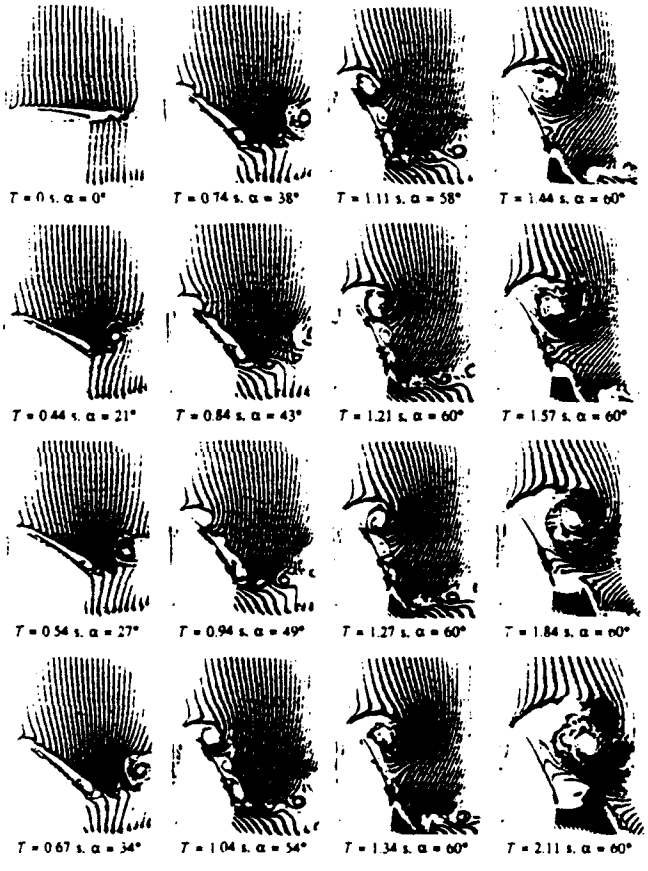

Fig. 2 Evolution of the flowfield on the airfoil suction surface ($\Omega^* = 0.4$, $e = 0.15$).

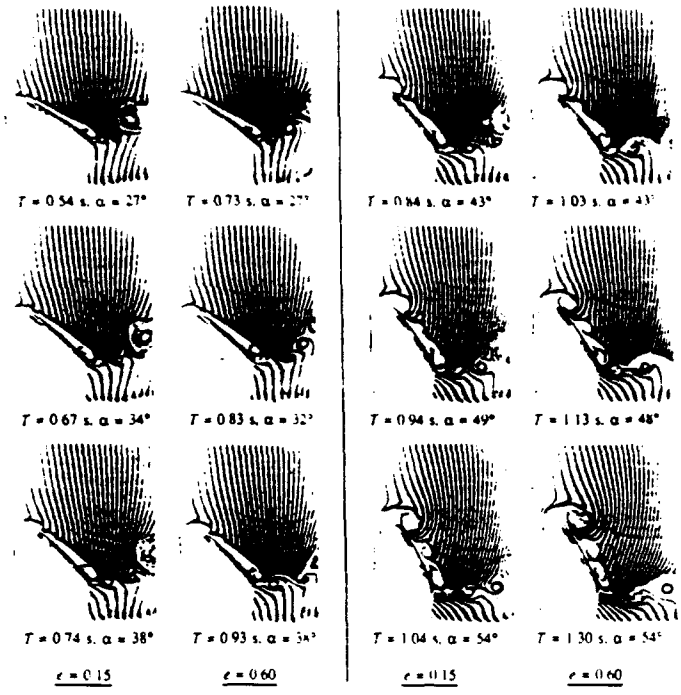

Fig. 3 Comparison of flow evolution for two different initial acceleration periods ($\Omega^* = 0.4$).

Table 1 Time and angle of attack at the onset of leading-edge separation

	T_s, s	α_s, deg
$\Omega^* = 0.4$; $e = 0.6$	0.80	31
$\Omega^* = 0.4$; $e = 0.15$	0.64	32
$\Omega^* = 0.4$; $e = 0.037$	0.57	31
$\Omega^* = 0.2$; $e = 0.15$	0.97	24
$\Omega^* = 0.2$; $e = 0.037$	0.90	25

The downstream convection of the dynamic stall vortex was determined for all of the cases from image sequences similar to Fig. 2. The vortex downstream position X (along freestream direction) was estimated using the center of the nearly circular region interpreted to be the signature of the dynamic stall vortex (e.g., see Fig. 2). The results are referenced to the fixed pitch axis location X_p and are plotted in Fig. 4. Note that the differences in the times for the onset of leading-edge separation among the various cases have been taken into account by using the relative time ($T - T_s$). The main result from Fig. 4 is that the initial acceleration period also has little influence on the downstream convection of the dynamic stall vortex for the cases studied. Note that the vortex convection speed U_c/U_∞ (determined from a least-squares straight line fit to data) is 0.44 and 0.40 for $\Omega^* = 0.4$ and 0.20, respectively.

To summarize, the results presented indicate that the elapsed time for the occurrence of various events is affected by the initial acceleration; the angle of attack where these events occur is practically unchanged, however. This includes the onset of leading-edge separation and many of the details of the dynamic stall vortex formation, downstream convection, and its interactions. These results imply that a convenient acceleration profile can be selected for experimental and computational studies without seriously impacting the dynamics of the unsteady stall process.

A scaling argument based on unsteady inviscid flow results had earlier suggested[10] that if the initial acceleration time scale is sufficiently short compared to the flow time scale, the onset

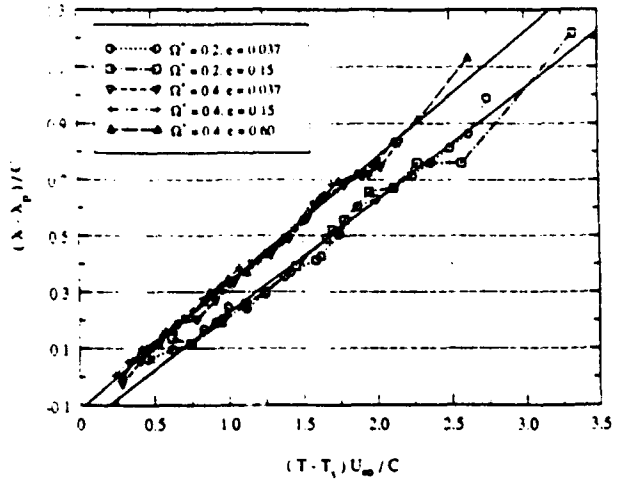

Fig. 4 Downstream convection of the dynamic stall vortex. Solid lines represent the least-squares line fit to data.

of leading-edge separation might be expected to be insensitive to the motion history, as is resported here. This is consistent with the constant pitch rate, inviscid flow, lift-curve slope results in Ref. 4 which indicate that at high enough pitch rates motion history effects will saturate. We should mention that in all of the cases studied here, the acceleration period was short enough that it ended before the onset of leading-edge separation. Reference 10 further suggests that initial acceleration effects may become important for a combination of low pitch rate Ω^* and long acceleration period ϵ.

We note that the results presented here only address the timing of the various events in the flowfield development. We do not know at this time how other important quantities such as the surface pressure gradient, surface vorticity flux, and the integrated load on the airfoil are affected as we change the acceleration period. These questions are currently being addressed by computing the flows discussed here using a two-dimensional Navier-Stokes solver. Preliminary computational results[11] corroborate the present findings.

Acknowledgments

This work was supported by the Air Force Office of Scientific Research Grants AFOSR-89-0417 and AFOSR-89-0130. Charles Gendrich is gratefully acknowledged for his help with the preparation of the manuscript.

References

[1]McCroskey, W. J., "Unsteady Airfoils," *Annual Review of Fluid Mechanics*, Vol. 14, 1982, pp. 285-311.

[2]Carr, L. W., "Progress in Analysis and Prediction of Dynamic Stall," *Journal of Aircraft*, Vol. 25, No. 1, 1988, pp. 6-17.

[3]Francis, M. S., and Keesee, J. E., "Airfoil Dynamic Stall Performance with Large-Amplitude Motions," *AIAA Journal*, Vol. 23, No. 11, 1985, pp. 1653-1659.

[4]Jumper, E. J., Shreck, S. J., and Dimmick, R. L., "Lift-Curve Characteristics for an Airfoil Pitching at Constant Rate," *Journal of Aircraft*, Vol. 24, No. 10, 1987, pp. 680-687.

[5]Lorber, P. F., and Carta, F. O., "Airfoil Dynamic Stall at Constant Pitch Rate and High Reynolds Number," *Journal of Aircraft*, Vol. 25, No. 6, 1988, pp. 548-556.

[6]Visbal, M. R., "On the Formation and Control of the Dynamic Stall Vortex on a Pitching Airfoil," AIAA Paper 91-0006, Jan. 1991.

[7]Ghia, K. N., Yang, J., Osswald, G. A., and Ghia, U., "Study of the Dynamic Stall Mechanism Using Simulation of Two-Dimensional Navier-Stokes Equations," AIAA Paper 91-0546, Jan. 1991.

[8]Acharya, M., and Metwally, M. H., "Unsteady Pressure Field and Vorticity Production over a Pitching Airfoil," *AIAA Journal*, Vol. 30, No. 2, 1992, pp. 403-411.

[9]Shih, C., Lourenco, L., Van Dommelen, L., and Krothapalli, A., "Unsteady Flow Past an Airfoil Pitching at Constant Rate," *AIAA Journal*, Vol. 30, No. 5, 1992, pp. 1153-1161.

[10]Koochesfahani, M. M., Smiljanovski, V., and Brown, T. A., "Effect of Initial Acceleration on the Flow Development of the Flow Field of an Airfoil Pitching at Constant Rate," *Proceedings of NASA/AFOSR/ARO Workshop on Physics of Forced Unsteady Separation*, NASA Ames Research Center, April 17-19, 1990, NASA CP 3144, 1992, pp. 317-332.

[11]Gendrich, C. P., Koochesfahani, M. M., and Visbal, M. R., "Initial Acceleration Effects on the Flow Field Development around Rapidly Pitching Airfoils," AIAA Paper 93-0438, Jan. 1993.

Decay of Aircraft Vortices near the Ground

Milton E. Teske* and Alan J. Bilanin†
Continuum Dynamics, Inc., Princeton, New Jersey 08543
and
John W. Barry‡
U.S. Department of Agriculture Forest Service, Davis, California 95616

Introduction

In a review of the state of knowledge of aircraft vortices, Donaldson and Bilanin[1] include a discussion on the effects of atmospheric turbulence on the aging of vortex pairs. One of the models suggested may be written

$$\Gamma(t) = \Gamma_o \exp\left(-\frac{bqt}{s}\right) \tag{1}$$

where Γ is the vortex circulation strength as a function of time t, Γ_o the initial vortex circulation strength at $t = 0$, b the decay coefficient, q the ambient turbulence level, and s the aircraft semispan.

Donaldson and Bilanin[1] invoke simple arguments to suggest that the decay coefficient—out of ground effect—may take a value of 0.41. When details about the wakes of large aircraft were first investigated (in the early 1970s), more sophisticated models, using various techniques such as second-order closure of the Reynolds stress equations,[2] were developed with an eye toward examining this decay behavior. Recently, for a completely different reason, the problem of quantifying the decay coefficient has produced a sizable field study and data examination.

Discussion

Between 1985 and 1991, a series of aircraft flybys above tower grids instrumented with propeller anemometers produced a large data base on vortex motion near the ground.[3] These tests were performed jointly by the United States Department of Agriculture Forest Service and the United States Army at several sites in northern California (through Project WIND), and at Dugway Proving Ground, Utah. Anemometer tower grids recorded the ambient vertical velocity time histories as various aircraft repeatedly traversed normal to the grid. These digitized velocity traces produced an aircraft wake signature that could be used to infer the strength and lateral and vertical motion of the aircraft vortex pairs generating the traces. Table 1 summarizes the complete data set.

The location and strength of the vortices traversing the anemometer tower grid may be inferred by a least-squares analysis defining an error E as

$$E = \sum_{n=1}^{N} (w_n - \bar{w}_n)^2 \tag{2}$$

Received Nov. 12, 1992; revision received Jan. 15, 1993; accepted for publication Feb. 5, 1993.

*Senior Associate, P.O. Box 3073.
†President and Senior Associate, P.O. Box 3073.
‡Pesticide Specialist, Forest Pest Management, 2121C Second Street, Suite 102.

APPENDIX B

Manuscript Submitted to the *Journal of Fluids Engineering.*

Effects of Initial Acceleration on the Flow Field Development around Rapidly Pitching Airfoils

C. P. Gendrich*, M. M. Koochesfahani†
Department of Mechanical Engineering
Michigan State University, E. Lansing, MI 48824

and

M. R. Visbal‡
CFD Research Branch, Aeromechanics Division, Wright Laboratory,
Wright-Patterson AFB, Dayton, OH 45433

Computational results are presented to show how the acceleration period at the start of constant pitch rate trajectories affects the dynamic stall process. Large amplitude motions were studied on the basis of an NACA 0012 airfoil pitching about the quarter-chord axis. Constant (ON/OFF) acceleration profiles, with non-dimensional acceleration periods ranging between 0.039 to 0.6, and large pitch rates ($0.1 \le \Omega^* \equiv \dot{\alpha}c/2U_\infty \le 0.4$) were used. The initial acceleration is observed to affect the integrated loads, surface pressure distribution, and the evolution of reversed flow regions just above the surface of the airfoil only during the acceleration period and for a relatively short time ($\tau \equiv tU_\infty/c \le 0.25$) afterwards. After that time, all of these quantities only depend on the instantaneous angle of attack for a given pitch rate. These conclusions are consistent with previous experimental flow visualization observations. The onset of leading edge separation at high and low pitch rates is shown to be characterized by different processes. At low pitch rates leading edge separation occurs after the reversed flow front originating at the trailing edge has reached the leading edge. At higher pitch rates leading edge separation and the upstream progression of the (trailing edge) reversed flow front develop independently.

Nomenclature

c	airfoil chord
DSV	dynamic stall vortex
DSVP	dynamic stall vortex suction peak at the surface
e	dimensionless acceleration rate, T_a/T_c
LESP	leading edge suction peak
M_∞	free stream Mach number
Re_c	Reynolds number based on chord length
S	distance along the airfoil surface
T_a	acceleration period
T_c	time required to pitch to 0°–60° when $T_a \to 0$
U_∞	free stream velocity
α	angle of attack
α_{sep}	α at the onset of leading edge separation
τ	dimensionless time, tU_∞/c
Ω^*	dimensionless pitch rate, $\dot{\alpha}c/2U_\infty$

* Graduate Student
† Associate Professor
‡ Aerospace Engineer

I. Introduction

The dynamic stall process has been under investigation for over a decade now, and significant progress has been made toward understanding the physical processes associated with rapidly pitching an airfoil beyond its static stall angle of attack. The reviews of McCroskey (1982), Carr (1988), and Visbal (1990) provide good descriptions of the dynamic stall process as it is currently understood. As the dynamic stall problem was first recognized for its relevance to helicopter performance, the first motion trajectories studied were sinusoidal in nature, and a reduced frequency $k \equiv \omega c/2U_\infty$ was defined as one of the controlling parameters.

More recently, constant pitch rate motions have received a great deal of attention for their application to supermaneuverable aircraft. These trajectories have an advantage over sinusoidal motions for those studying the physics of the problem, since they offer less complicated experiments with which to study the phenomena associated with dynamic stall. For constant pitch rate motions a non-dimensional pitch rate, $\Omega^* \equiv \dot{\alpha}c/2U_\infty$, has been introduced as one of the governing parameters. It is clear that the initial part of the motion trajectory is distinguished by a non-constant pitch rate motion due to the finite accelera-

tion period which is characteristic of a real device. Very little is known about the influence of this initial acceleration period on the subsequent flow development around airfoils pitching to high angles of attack.

In an experimental flow visualization study by Koochesfahani and Smiljanovski (1993), the initial acceleration was systematically varied in order to document its effects on flow development for constant, relatively high pitch rate motions. The motion trajectory consisted of a constant acceleration period followed by a constant pitch rate segment and finally a constant deceleration portion. The airfoil pitched from 0° to 60°; see Figure 1. The acceleration effects were described in terms of a non-dimensional acceleration period, $e \equiv T_a/T_c$, where T_a is the acceleration period and T_c refers to the time to pitch from 0° to 60° for the ideal (i.e., $T_a \rightarrow 0$) constant pitch rate motion. It was found that the angle of attack at the onset of leading edge separation was practically independent of the acceleration period. Furthermore, the subsequent flow developments after leading edge separation, such as the evolution of the dynamic stall vortex and its convection over the airfoil, were similarly insensitive to the details of the start of the motion. In all the cases studied, leading edge separation occurred after the initial acceleration period had ended. That investigation, which was qualitative and entirely based on flow visualization, only addressed the timing of the various events in the flow field development. The effects of initial acceleration on other important features of the flow, such as the integrated loads on the airfoil and the surface pressure gradient, have not yet been quantified.

All computational studies of nominally constant pitch rate motions also contain an initial acceleration phase. However, except for one preliminary investigation (Visbal, 1986), none of the previous studies has specifically addressed the effects of initial acceleration on the dynamic stall process. The current work, which is the computational counterpart of the flow visualization study of Koochesfahani and Smiljanovski (1993), aims to quantify the initial acceleration effects on the pitching airfoil flow field using two dimensional full Navier-Stokes computations. These effects are characterized here in terms of the computed flow visualizations, the integrated load on the airfoil, the surface pressure distributions, and the evolution of reversed flow fronts just above the airfoil surface.

II. Computational Procedure

The current computations are based on the Navier-Stokes solver of Visbal and Shang (1989). This code uses the implicit approximately-factored algorithm of Beam and Warming (1978) to solve the unsteady compressible form of the Navier-Stokes equations written in the strong conservation form. The usual forms of implicit and explicit nonlinear dissipation as described by Jameson, Schmidt and Turkel (1981) are employed in order to ensure numerical stability. Further details can be found in Visbal and Shang (1989).

The computational parameters were selected to allow comparison with the range of experimental conditions in the water tunnel studies of Koochesfahani and Smiljanovski (1993) and Brown (1992). The computed flow field was that of an NACA 0012 airfoil pitching about the quarter-chord axis from zero to 60° angle of attack, α. The freestream Mach number was 0.1, and the chord Reynolds number was 12,000. The maximum density variation was less than 3% for this Mach number, which should enable acceptable comparisons to be made with previous water tunnel studies. Pitch rates in the range $0.1 \le \Omega^* \le 0.4$ were computed with acceleration values in the range $0.001 \le e \le 0.6$. In this paper results will be presented only for $\Omega^* = 0.1$, 0.2, and 0.4 with $e = 0.6$, 0.15, and 0.039. The entire computational flow field was stored every ½° from 0° through 50°. The flow was expected to be laminar, at least during the initial phase of the separation process, so a turbulence model was not required.

Particle tracking was added to the code for this study, so that the computational results could be compared directly with experimental hydrogen bubble flow visualizations. A fixed number of "particles" was introduced into the computational domain, and their positions were advanced using a first-order marching scheme. The particles were given initial locations in space such that they simulated lines of hydrogen bubbles from a pulsed wire. Gendrich, Koochesfahani, and Visbal (1992) have shown a very good correspondence between these computed "flow visualizations" and those obtained experimentally. In addition, the visual appearance of a "bulge" near the nose of the airfoil at the onset of leading edge separation correlates strongly with changes in the character of the vorticity field and the tangential velocity just above the airfoil's surface.

Results and Discussion

Koochesfahani and Smiljanovski (1993) observed that varying the initial acceleration period did not seem to affect the visual appearance of the dynamic stall process. In Figure 2 we present a com-

parison between their experimental and our computed flow visualizations for $\Omega^* = 0.4$ at various angles of attack, illustrating the onset of leading edge separation for two different accelerations. There are many more hydrogen bubbles in the experimental flow field than particles in our computed domain, which accounts for the more continuous appearance of the experimental visualizations. Nevertheless, the computations reveal the presence of essentially the same features developing above the surface of the airfoil. At 27° the flow near the leading edge is seen to follow the contour of the airfoil, and to that extent exhibits the behavior of an attached flow. At 34° a "bulge" has formed near the leading edge, and visually we could identify the onset of leading edge separation to have occurred at an angle, α_{sep}, somewhere between 27° and 34°. Based on the computed flow visualization time series, α_{sep} was determined to be approximately 33½°. As the airfoil pitches to higher angles of attack, the bulge develops into the dynamic stall vortex (DSV), while secondary vortex rollup and pairing occurs over the aft portion of the airfoil. The computational results shown in Figure 2 indicate that the onset of leading edge separation is not influenced by the initial acceleration, in agreement with the experimental observations.

To quantify the initial acceleration effects, we first discuss the behavior of the integrated loads on the airfoil. The computed lift, drag, and moment curves for $\Omega^* = 0.4$ are shown in Figure 3. The spiky overshoots near the beginning of each curve are believed to be due to apparent mass effects. The important result is that each force coefficient approaches a curve which depends only on the instantaneous angle of attack (i.e., is independent of e) within a time scale of $\tau = 0.26$ after the end of the acceleration period (see Table 1); τ is the non-dimensional time defined by $\tau \equiv tU_\infty/c$. For the particular pitch rate considered in Figure 3, this time scale corresponds to a maximum change in the angle of attack of 10° beyond the end of acceleration. The sudden change in the behavior of the force coefficients at 42° for the case of $e = 0.6$ is due to the beginning of the deceleration period for that case.

Figures 4 and 5 show the lift, drag, and moment coefficients versus angle of attack for $\Omega^* = 0.2$ and 0.1, respectively. The same acceleration effects are observed as for the higher pitch rate, namely, within $\tau = 0.25$ after the end of the acceleration period, the force coefficients have become independent of acceleration history. Comparisons with the experiments of Graham and Strickland (1986), Francis and Keesee (1985), and the computations of Ghia, Yang, Osswald, and Ghia (1991) are included in Figures 4 and 5. Overall agreement with the experiments is quite good; variations are probably due to differences in airfoil type, Reynolds number, and freestream Mach number.

e	Acceleration ends at:
0.039	$\alpha = 1.2°$
0.15	$\alpha = 4.5°$
0.60	$\alpha = 18.0°$

Table 1. Angle of attack at which acceleration ends. Note that these angles are independent of pitch rate for constant acceleration motion profiles. Deceleration begins at 42° for $e = 0.60$.

Since the integrated loads are primarily the result of the surface pressure distribution, and leading edge separation is connected to the surface pressure gradient, the effects of acceleration history on the development of the surface pressure and pressure gradient profiles are presented next. The typical evolution of these profiles at a fixed value of initial acceleration, e, is first illustrated in Figures 6 and 7. Note the formation of the leading edge suction peak (LESP) and its associated adverse pressure gradient, followed by the formation of the dynamic stall vortex peak (DSVP).[1] The first indication of DSVP formation occurs between 16° and 18.5°. The DSVP magnitude is initially less than that of the LESP, but it grows in strength and finally exceeds the leading edge suction peak. While the LESP remains practically fixed at a location near the leading edge, the DSVP moves toward the trailing edge at a fairly constant rate. The development of the pressure field displayed in Figures 6 and 7 agrees very well with that presented by Acharya and Metwally (1992), Visbal (1991), and others.

The effects of varying the initial acceleration on the development of the surface pressure distribution are illustrated in Figures 8-12. Results are shown for two pitch rates at selected angles before and after the onset of leading edge separation. The evolution for the lower pitch rate ($\Omega^* = 0.1$) at $\alpha = 3°$, 16° (before α_{sep}), and 20° (after α_{sep}) is presented in Figures 8-10. At 3° the acceleration has already ended for $e = 0.039$, while it continues for the other two e values. The pressure over practically the entire surface is different for each value of e, with the exception of

[1] The DSVP refers to the pressure minimum at the *airfoil surface*, and not the pressure minimum in the core of the dynamic stall vortex. This definition of the DSVP is the same as that used by Acharya and Metwally (1992).

the stagnation region. Note, however, that the pressure gradient shows much less sensitivity to variations in e. Similar behavior of the surface pressure gradient is exhibited at $\alpha = 16°$, just before the formation of the DSVP; note that by this angle of attack the surface pressure profile has relaxed to a single curve nearly independent of the variations in e. This lack of sensitivity by the surface pressure gradient to the initial acceleration history is responsible for the corresponding insensitivity of the leading edge separation angle observed experimentally and computationally.

After acceleration has ended for all three cases and leading edge separation has begun (Figure 10, $\alpha = 20°$), even the surface *pressure* field exhibits an insensitivity to e, similar to that shown by the surface pressure *gradient*. This similarity among the different acceleration cases for both the surface pressure and gradient is consistent with the previous experimental observations indicating that the subsequent development of the dynamic stall flow field is not influenced by the initial acceleration history for the range of parameters investigated. Figures 11 and 12 showing the pressure field before and after α_{sep} for the higher pitch rate of $\Omega^* = 0.4$ support all the assertions made earlier. For this pitch rate the pressure field exhibits even less dependence on initial motion history as compared to the $\Omega^* = 0.1$ case. It should be noted that the discussion presented here refers to the behavior of the surface pressure field over the first 30% of the chord (see Figs. 8-12). There are differences in the pressure field in the aft region of the airfoil which are responsible for the variation in the loads among the different cases; see Figs. 4 and 5. These differences do not have a significant influence on leading edge separation.

The discussion above addresses the flow behavior for only selected angles of attack. The evolution of the surface pressure field for the entire motion has been analyzed in Gendrich, Koochesfahani, and Visbal (1993) in terms of the magnitude and location of the various surface pressure minima and pressure gradient maxima corresponding to the LESP and DSVP evolution. The main conclusion from these results (not shown here) is that the effects of initial acceleration are limited to a short period (no more than $\tau = 0.25$) after the end of acceleration. In general, the development of the pressure gradient maxima is affected less than the evolution of the pressure minima, and the minimum pressure magnitude is less sensitive to acceleration history than its location. After a certain angle of attack ($\alpha = 6°$ for $\Omega^* = 0.1$, $\alpha = 8°$ for $\Omega^* = 0.2$, and $\alpha = 10°$ for $\Omega^* = 0.4$) the magnitudes and locations for both the pressure minima and pressure gradient maxima become independent of initial motion history and depend, for each pitch rate, only on the instantaneous angle of attack.

One of the prominent features of the unsteady separation process on a pitching airfoil is the existence of a thin region of reversed flow over the suction surface of the airfoil. The evolution of this reversed flow is believed to be intimately connected with the leading edge separation process. The effect of the initial acceleration on the development of various regions of reversed tangential flow in the rotating frame of the airfoil is characterized in Figure 13 for three different pitch rates. For each case, the progression of the reversed flow originating at the trailing edge has been labeled (1), and that which results from the vorticity concentration corresponding to the dynamic stall vortex has been labeled (2). Other regions of flow reversal are also shown in this figure; they correspond to other concentrations of vorticity (vortex roll-ups) existing over the upper surface.

Figure 13 (a), $\Omega^* = 0.1$, illustrates that the front of the reversed flow region labeled (1) begins near the trailing edge and moves upstream. When this front nears the leading edge ($\alpha = 20°$), a new region of forward flow labeled (2) forms, marking the occurrence of leading edge separation. It is very important to note that this behavior is quite different at higher pitch rates; see for example Figure 13 (c) for $\Omega^* = 0.4$. In this case the progression of the reversed flow front originating at the trailing edge never nears the leading edge (it only reaches $S/c = 0.3$) before leading edge separation is observed (as indicated by contour (2)). For this higher pitch rate a separate region of reversed flow labeled 3 develops near the leading edge at approximately 20°. Experimental evidence for this occurrence of leading-edge reverse flow independent of the trailing-edge reverse flow has recently been provided by Acharya (private communication).

As far as the initial acceleration effects are concerned, a longer acceleration period (e.g., $e = 0.6$) appears to speed the growth of the reversed-flow region from the trailing edge toward the leading edge. However, the important result from figure 13 is that, regardless of which of the two processes described above is characteristic of the flow (i.e., leading edge stall versus trailing edge stall), the initial acceleration does not significantly influence that process.

IV. Conclusions

The unsteady flow field around an NACA 0012 airfoil pitching to large angles of attack was presented

for three different pitch rates, $\Omega^* = 0.1$, 0.2, and 0.4, and three different initial constant acceleration periods, $e = 0.039$, 0.15, and 0.6. These are moderately large pitch rates for which leading edge separation begins after the acceleration has ended; no cases have been considered for which the airfoil was still accelerating at the onset of leading edge separation. The computational parameters were selected to allow comparison with earlier experimental studies.

The computed flow visualizations support the conclusions reached by the experimental observations of Koochesfahani and Smiljanovski (1993) that the onset of leading edge separation and the subsequent development of the dynamic stall vortex is not influenced by the initial motion history for the range of parameters studied. The present computations provide detailed quantitative information, not available from those experiments, about the integrated loads, surface pressure distributions, and the evolution of reversed flow regions just above the surface of the airfoil. The results show that the initial acceleration impacts these quantities only during the acceleration period and for a relatively short time ($\tau \leq 0.25$) afterwards. After that time, all of these quantities only depend on the instantaneous angle of attack for a given pitch rate. These findings are in qualitative agreement with the inviscid flow lift-curve slope results of Jumper, Shreck, and Dimmick (1987) which indicate that at high enough pitch rates motion history effects will saturate. We draw attention to the important implication of our results that a convenient acceleration profile can be selected for experimental and computational studies without seriously impacting the dynamics of the unsteady stall process.

The results presented also demonstrate that two different processes characterize the onset of leading edge separation at high and low pitch rates. At low pitch rates the onset of leading edge separation occurs after the reversed flow front originating at the trailing edge has reached the leading edge. At higher pitch rates, these two features develop independently; leading edge separation occurs without the reversed flow front from the trailing edge having ever reached the leading edge region.

Acknowledgements

We would like to acknowledge the support of the U. S. Air Force which provided computational resources and funding through grants AFOSR-89-0417 and F49620-86-C-0127.

References

1. McCroskey, W. J., "Unsteady airfoils," *Annual Review of Fluid Mechanics*, Vol. 14, 1982.

2. Carr, Lawrence W., "Progress in analysis and prediction of dynamic stall," *Journal of Aircraft*, Vol. 25, No. 1, 1988.

3. Visbal, M. R., "On some physical aspects of airfoil dynamic stall," *Proceedings of the ASME Symposium on Non-Steady Fluid Dynamics*, June 4-7, 1990.

4. Koochesfahani, M. M. and Smiljanovski, V., "Initial acceleration effects on flow evolution around airfoils pitching to high angles of attack," to appear in *AIAA Journal* in July, 1993.

5. Visbal, M. R., "Evaluation of an Implicit Navier-Stokes Solver for some Unsteady Separated Flows," *AIAA Paper* 86-1053, May, 1986.

6. Visbal, M. R. and Shang, J. S., "Investigation of the flow structures around a rapidly pitching airfoil," *AIAA Journal*, Vol. 27, No. 8, 1989.

7. Beam, R. M. and Warming, R. F., "An implicit factored scheme for the compressible Navier-Stokes equations," *AIAA Journal*, Vol. 16, No. 4, 1978.

8. Jameson, A., Schmidt, W., and Turkel, E., "Numerical solutions of the Euler equations by finite volume methods using Runge-Kutta time stepping schemes," *AIAA Paper* 81-1259, 1981.

9. Brown, T. A., "Effects of motion history on leading edge separation for an airfoil pitching to large angles of attack," *M. S. thesis*, Michigan State University, 1992.

10. Gendrich, C. P., Koochesfahani, M. M., and Visbal, M. R., "The visual and vortical signature of leading edge separation," *Bulletin of the American Physical Society*, Vol. 37, No. 8, 1992.

11. Graham, G. M. and Strickland, J. H., "An experimental investigation of an airfoil pitching at moderate to high rates to large angles of attack," *AIAA Paper* 86-0008, 1986.

12. Francis, M. S. and Keesee, J. S., "Airfoil dynamic stall performance with large-amplitude motions," *AIAA Journal*, Vol. 23, No. 11, 1985.

13. Ghia, K. N., Yang, J., Osswald, G. A., and Ghia, U., "Study of dynamic stall mechanism using simulation of two-dimensional unsteady Navier-Stokes equations," *AIAA Paper* 91-0546, 1991.

14. Acharya, M. and Metwally, M. H., "Unsteady pressure field and vorticity production over a pitching airfoil," *AIAA Journal*, Vol. 30, No. 2,

1992.

15. Visbal, M. R., "On the formation and control of the dynamic stall vortex on a pitching airfoil," *AIAA Paper* 91-0006, 1991.

16. Gendrich, C. P., Koochesfahani, M. M., and Visbal, M. R., "Initial acceleration effects on the flow field development around rapidly pitching airfoils," *AIAA Paper* 93-0438, 1993.

17. Jumper, E. J., Shreck, S. J., and Dimmick, R. L., "Lift-curve characteristics for an airfoil pitching at constant rate," *Journal of Aircraft*, Vol. 24, No. 10, 1987.

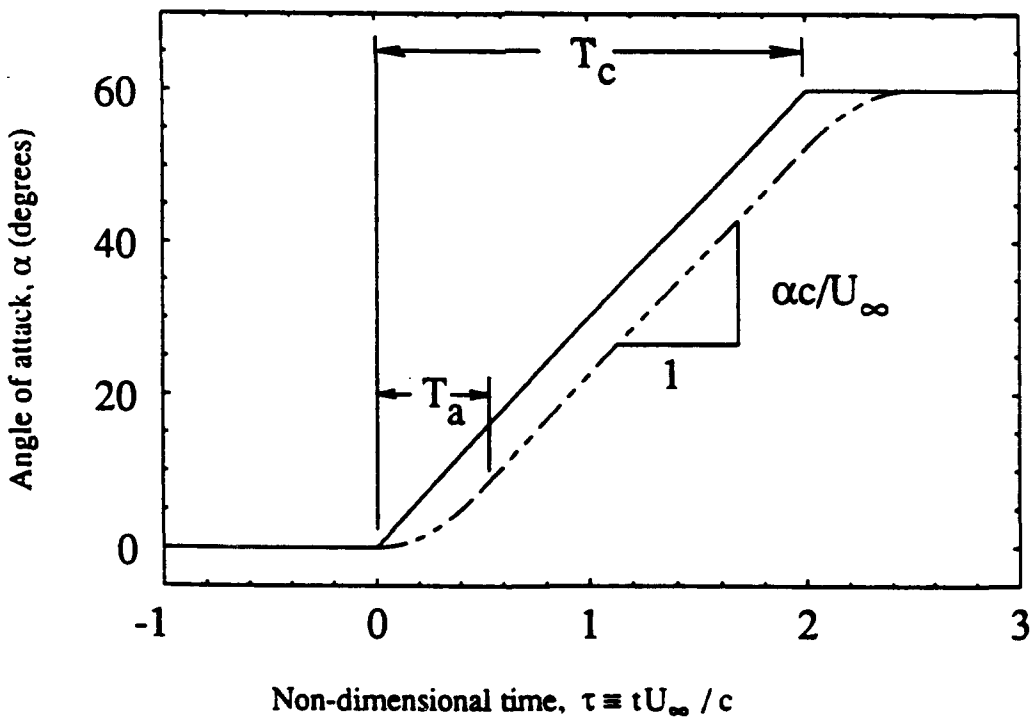

Figure 1. Ideal and typical motion profiles. $e \equiv T_a / T_c$ and $\Omega^* \equiv \dot{\alpha}c/2U_\infty$

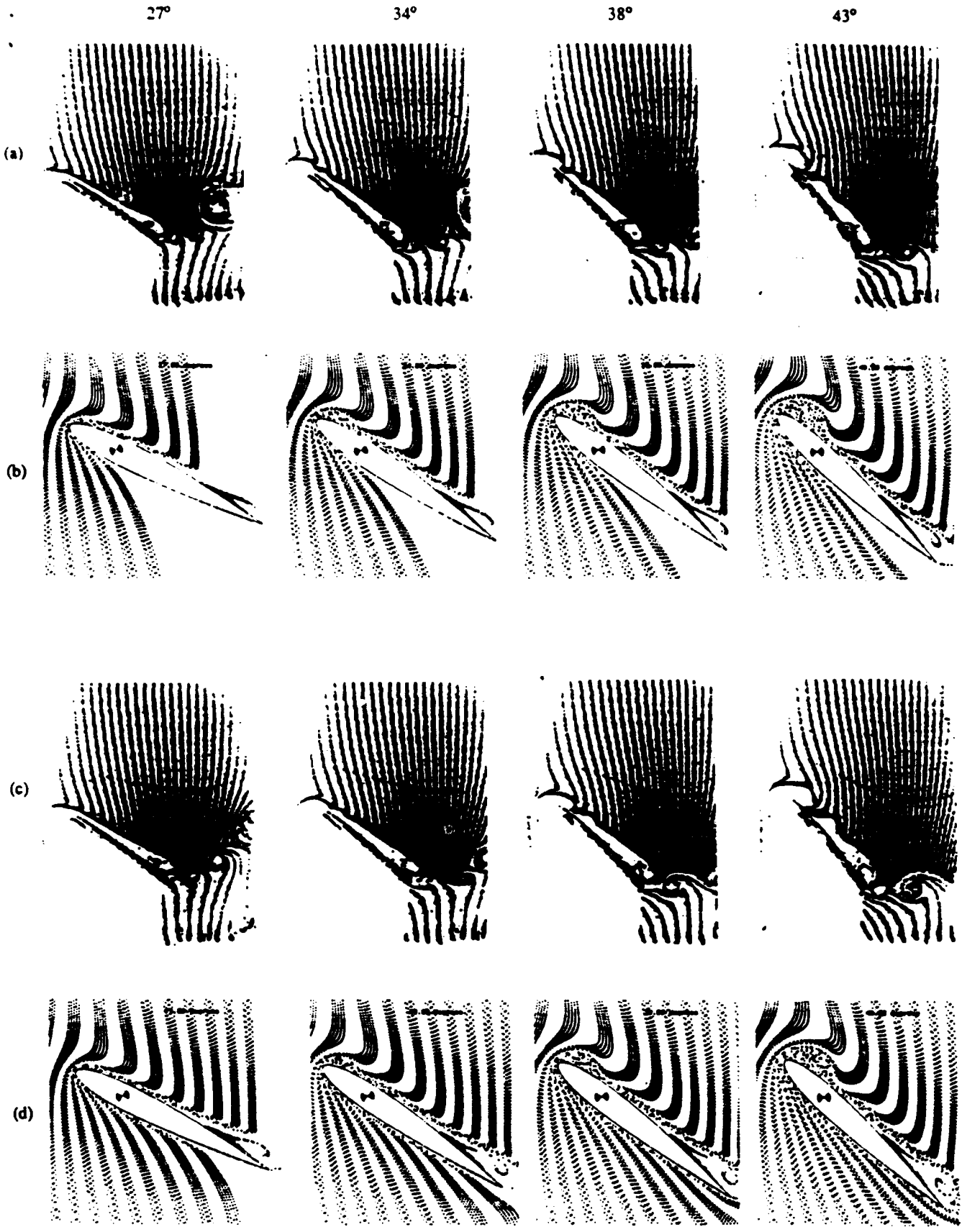

Figure 2. Experimental and computational flow visualizations for $\Omega^* = 0.4$ and two different accelerations. a) experiments, e=0.15; b) computations, e=0.15; c) experiments, e=0.60; and d) computations, e=0.60. Experimental flow visualizations are from Koochesfahani and Smiljanovski (1993).

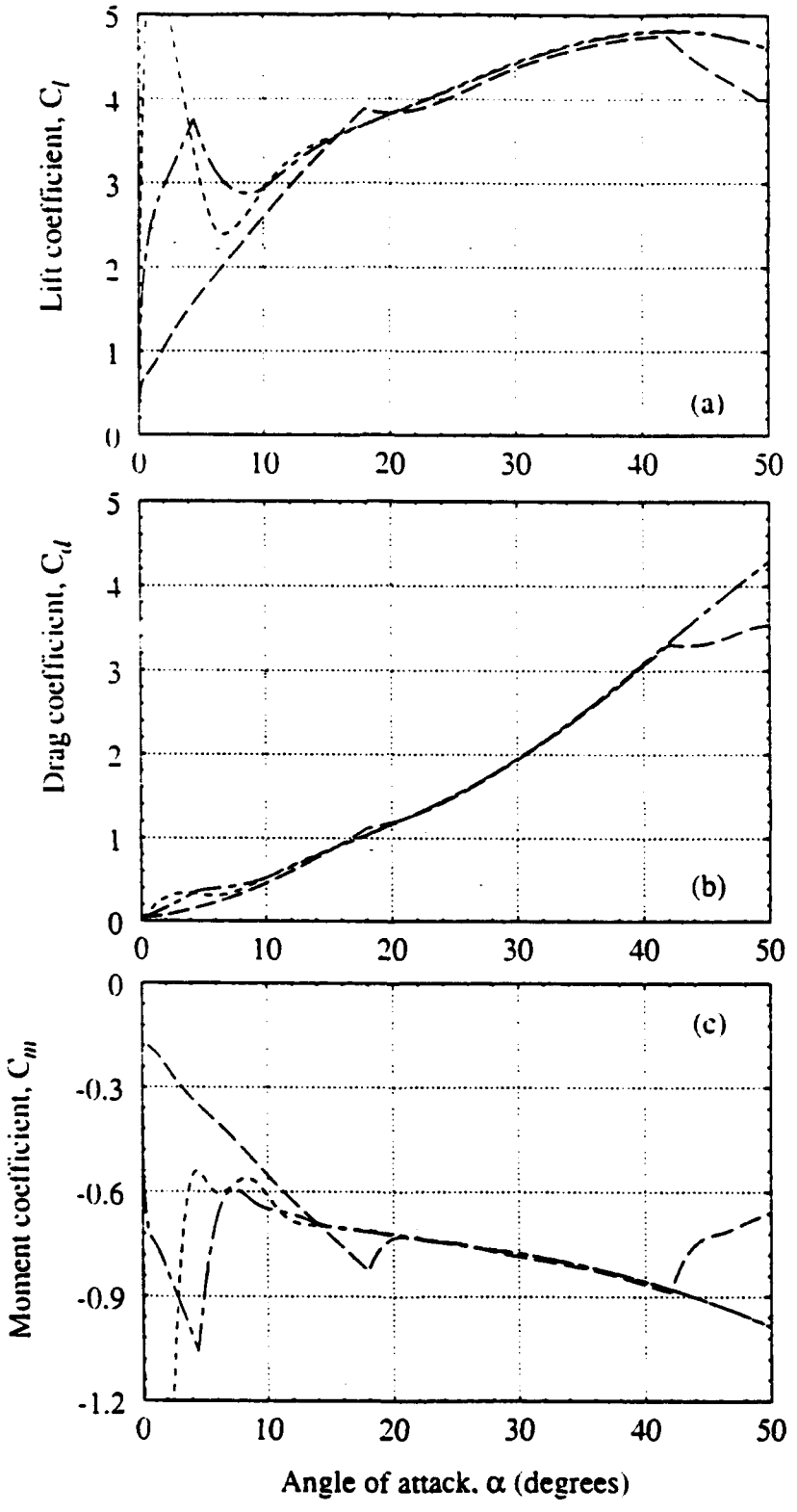

Figure 3. a) Lift, b) Drag, and c) Moment coefficients, $\Omega^* = 0.4$. ..... e = 0.039, —·— e = 0.15, and – – – – e = 0.60.

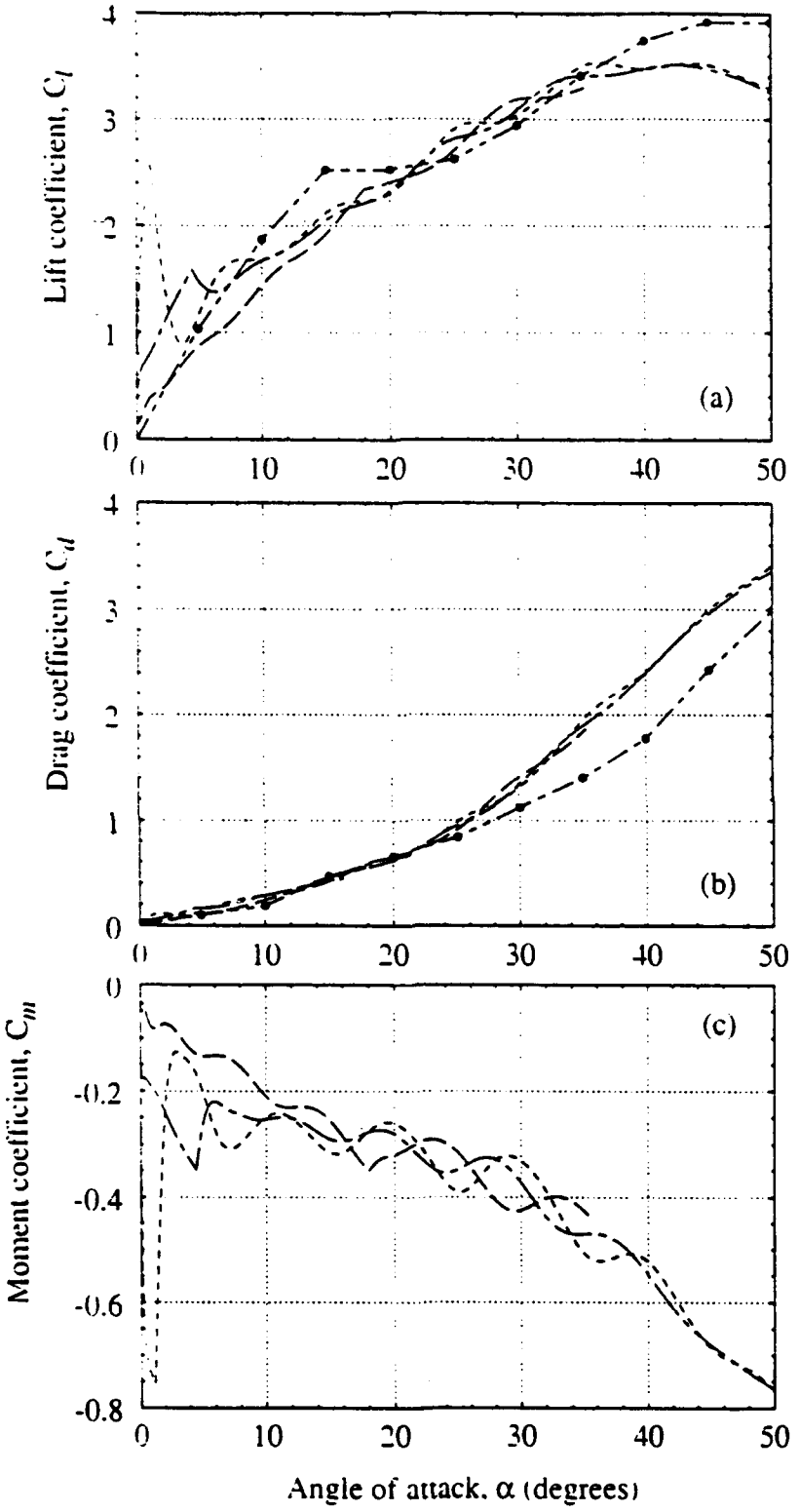

Figure 4. a) Lift, b) Drag, and c) Moment coefficients. $\Omega^* = 0.2$. ..... e = 0.039, —·— e = 0.15, – – – – e = 0.60, and •·····• Graham and Strickland (1986)

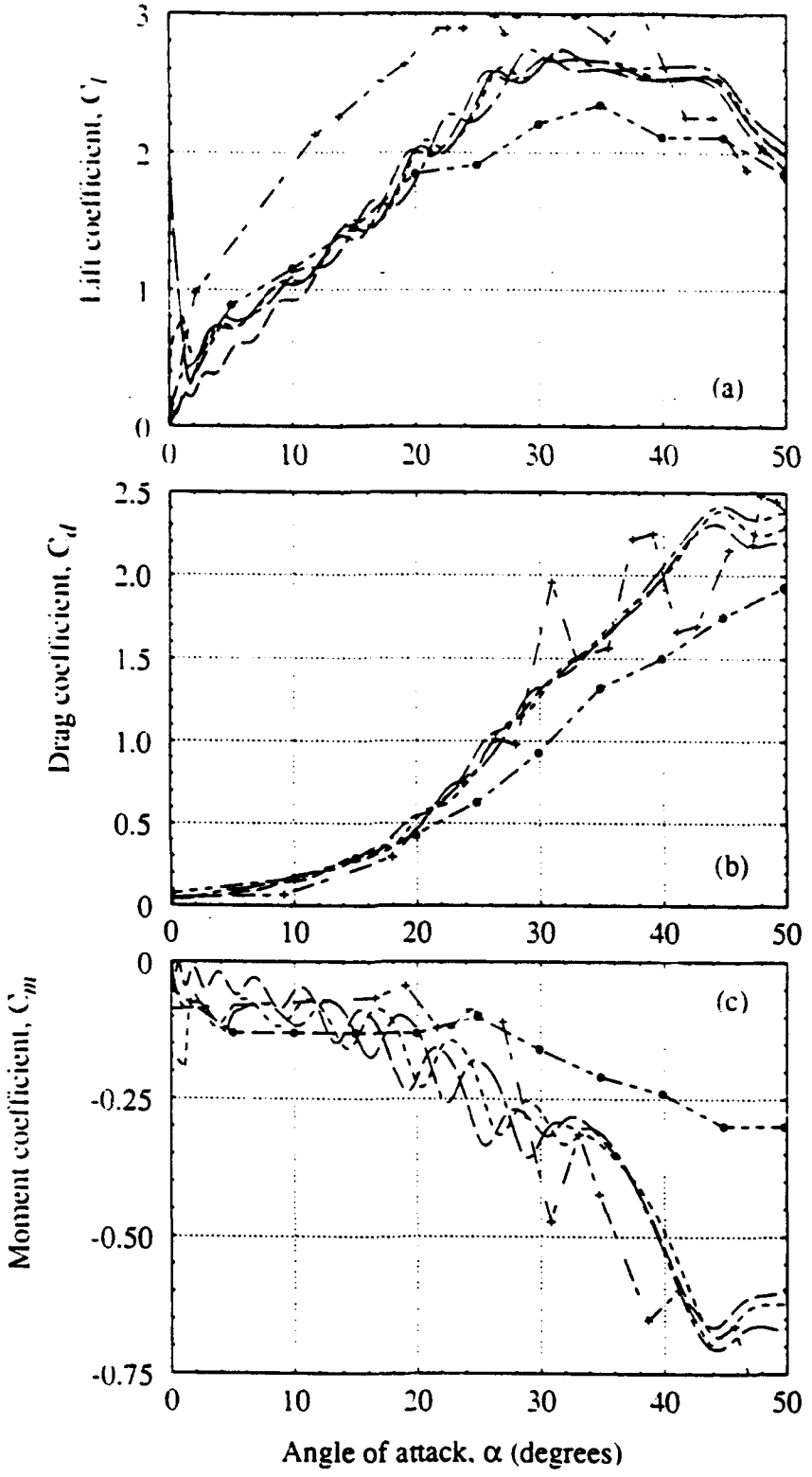

Figure 5. a) Lift, b) Drag and c) Moment coefficients, $\Omega^* = 0.1$. ..... e = 0.039, —·— e = 0.15, – – – – e = 0.60, •——• Francis and Keesee (1985), and ·–· ·–· Ghia, et al. (1991).

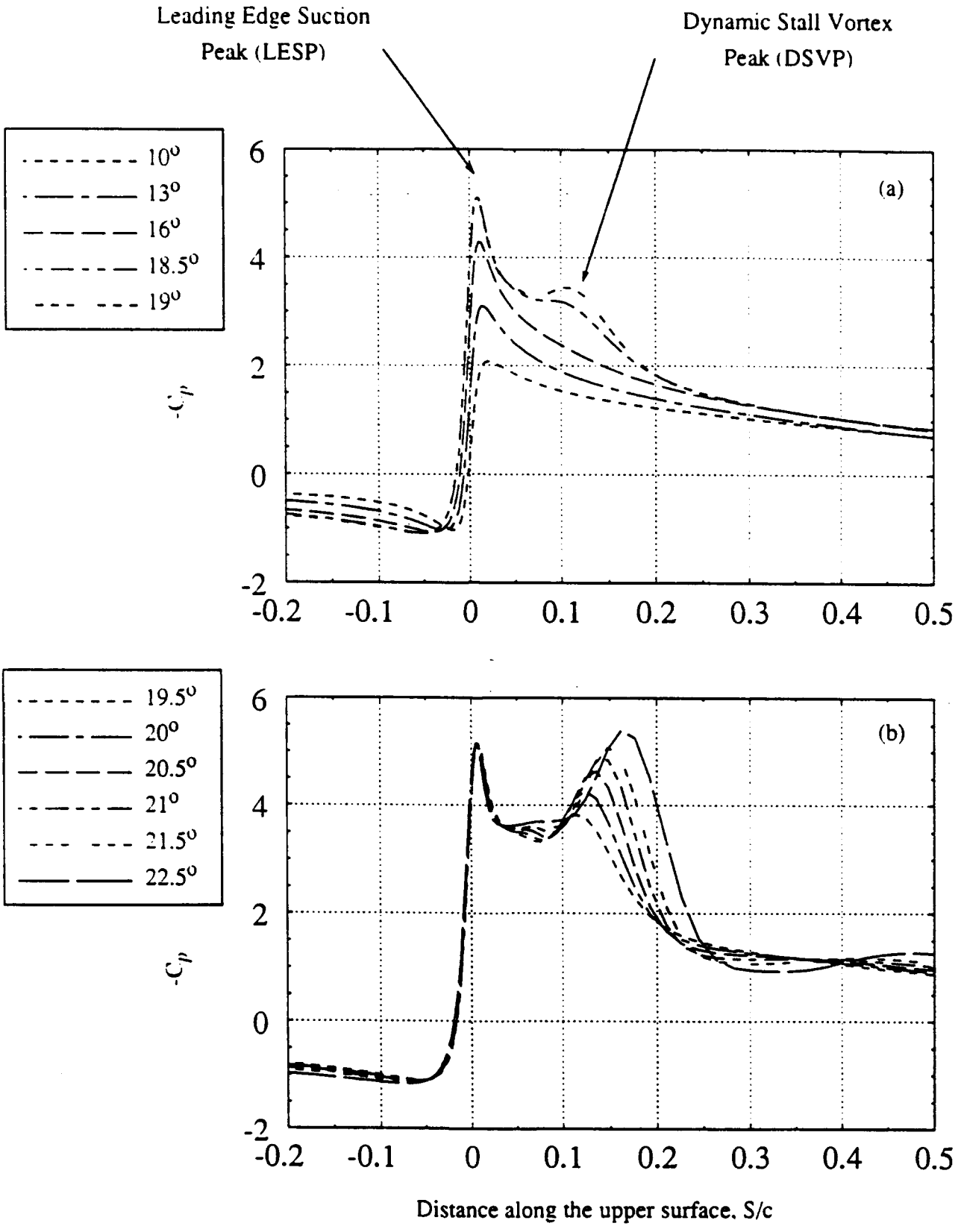

Figure 6. Development of the surface pressure profile during a dynamic stall event, $\Omega^* = 0.1$, e = 0.15: a) inception and b) growth of the dynamic stall vortex peak (DSVP)

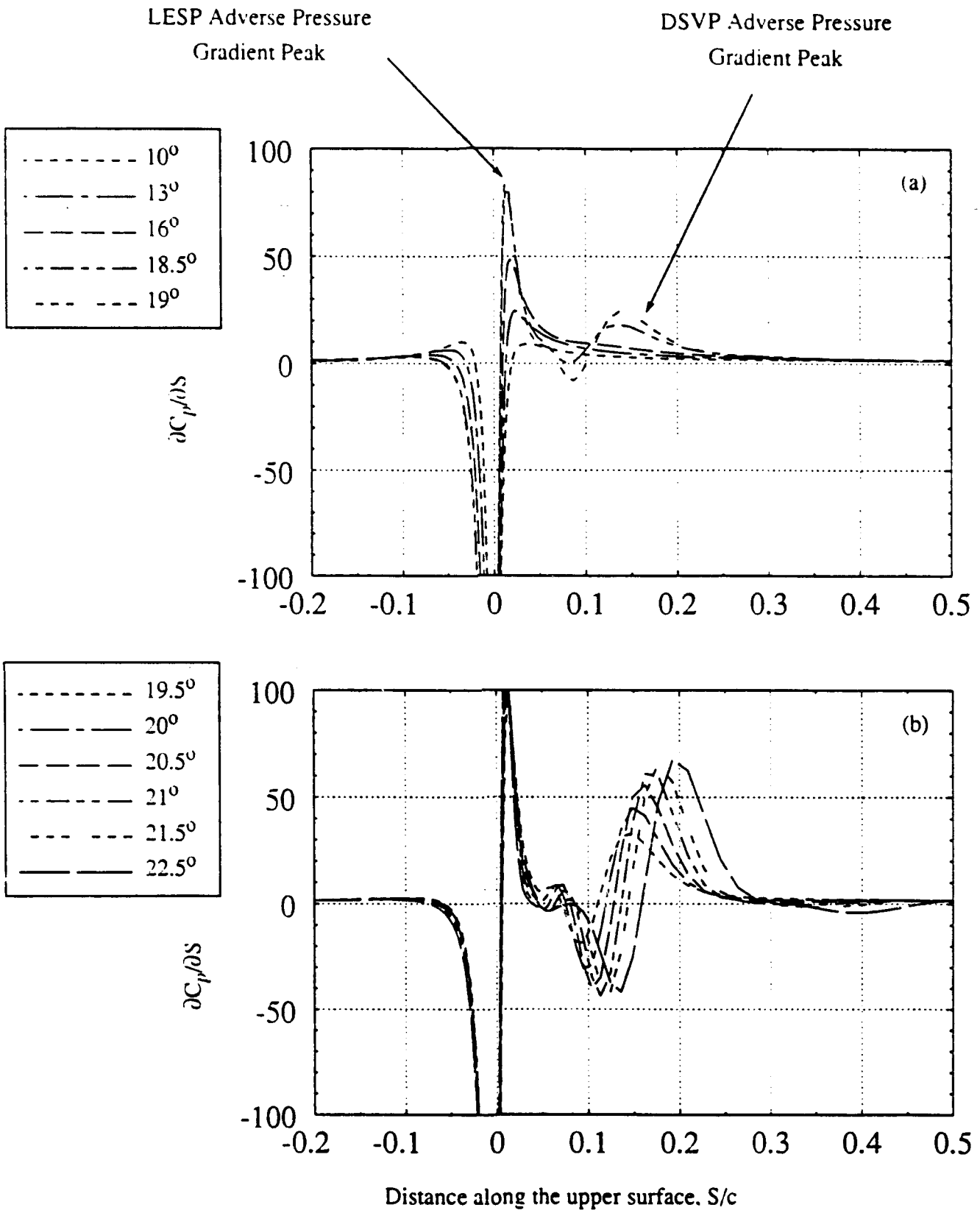

Figure 7. Surface pressure gradient evolution during a dynamic stall event. $\Omega^* = 0.1$, e = 0.15. Angles are the same as in Figure 6 a) and b).

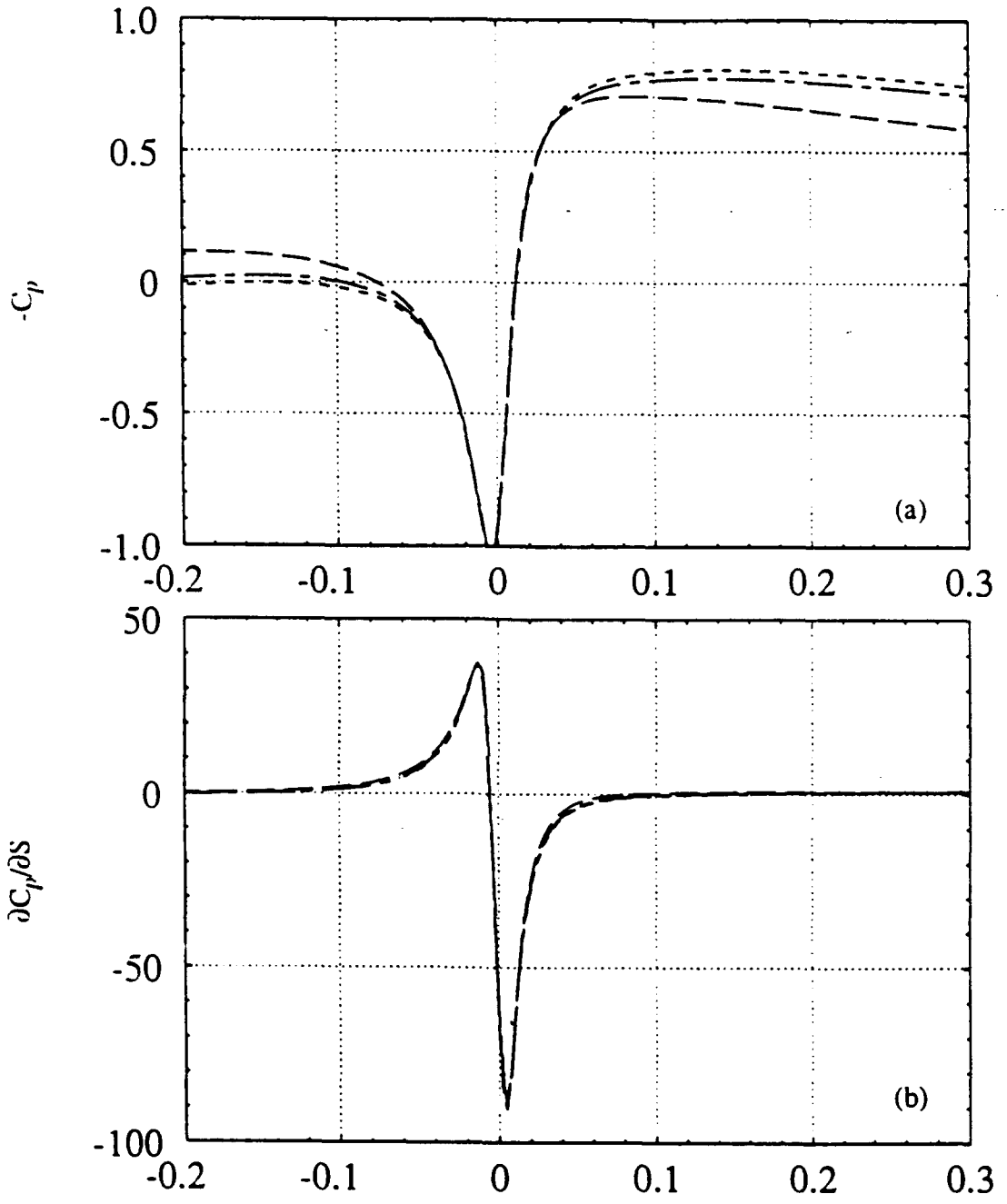

Figure 8. a) Surface pressure and b) surface pressure gradient profiles at 3°. $\Omega^* = 0.1$. Acceleration has ended for only the e = 0.039 trajectory. ..... e = 0.039, —·— e = 0.15, and – – – e = 0.60.

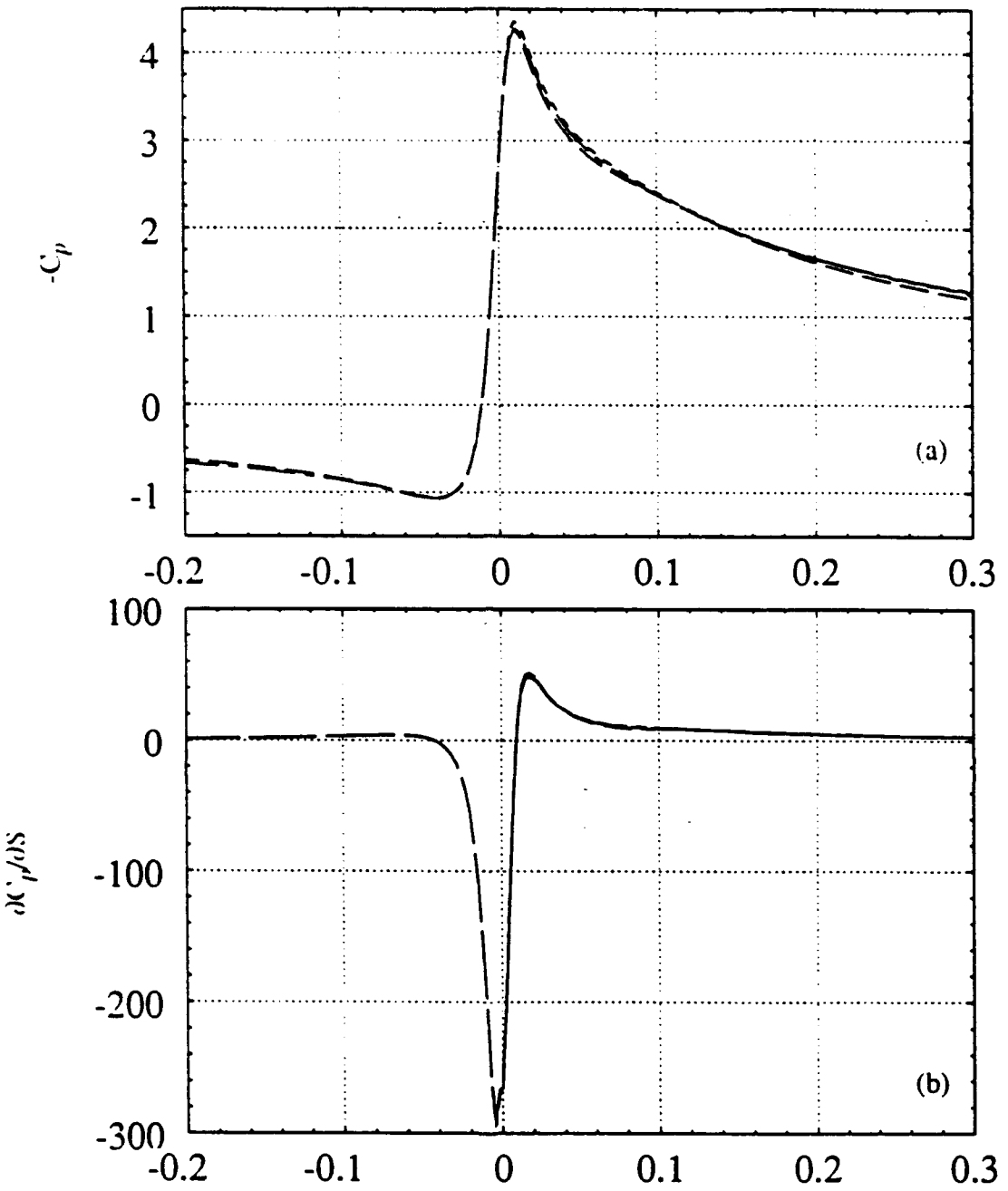

Figure 9. a) Surface pressure and b) surface pressure gradient profiles just before the onset of leading edge separation (16^o). $\Omega^* = 0.1$. ..... e = 0.039. —·— e = 0.15, and ---- e = 0.60.

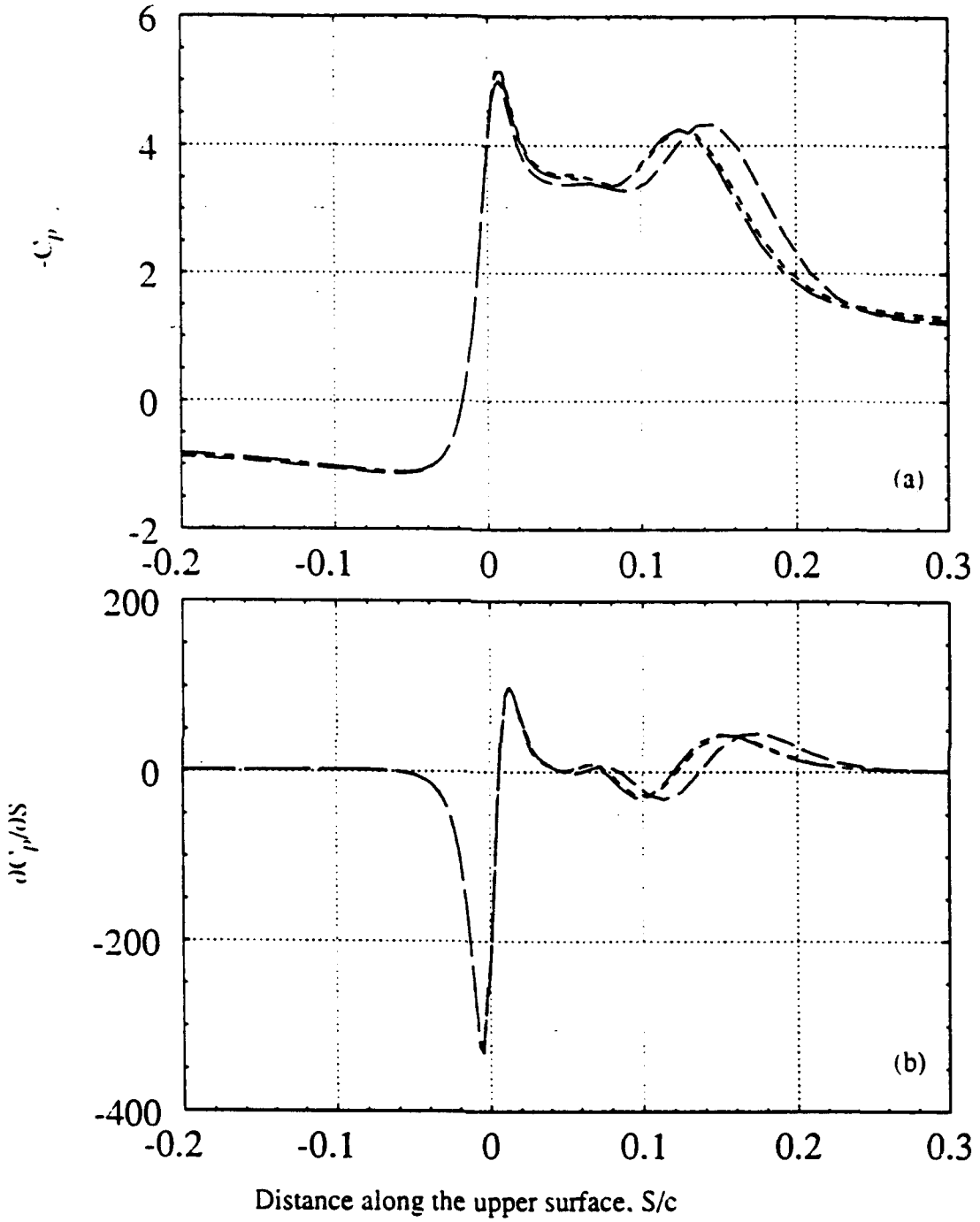

Figure 10. a) Surface pressure and b) surface pressure gradient profiles just after the onset of leading edge separation (20°). $\Omega^* = 0.1$. ..... e = 0.039. —·— e = 0.15. and ---- e = 0.60.

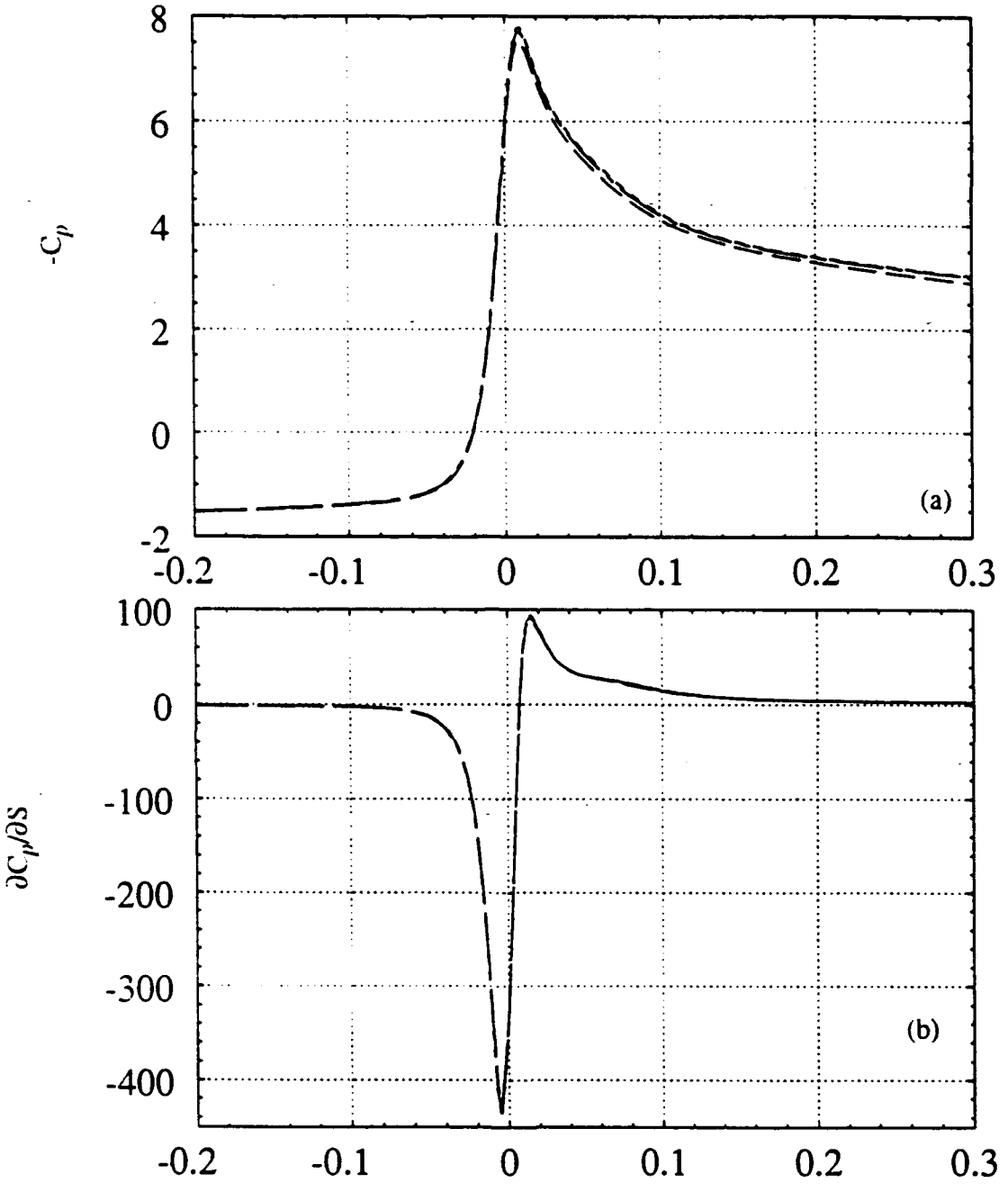

Figure 11. a) Surface pressure and b) surface pressure gradient profiles just before the onset of leading edge separation (22°). $\Omega^* = 0.4$. ..... e = 0.039, —·— e = 0.15, and – – – – e = 0.60.

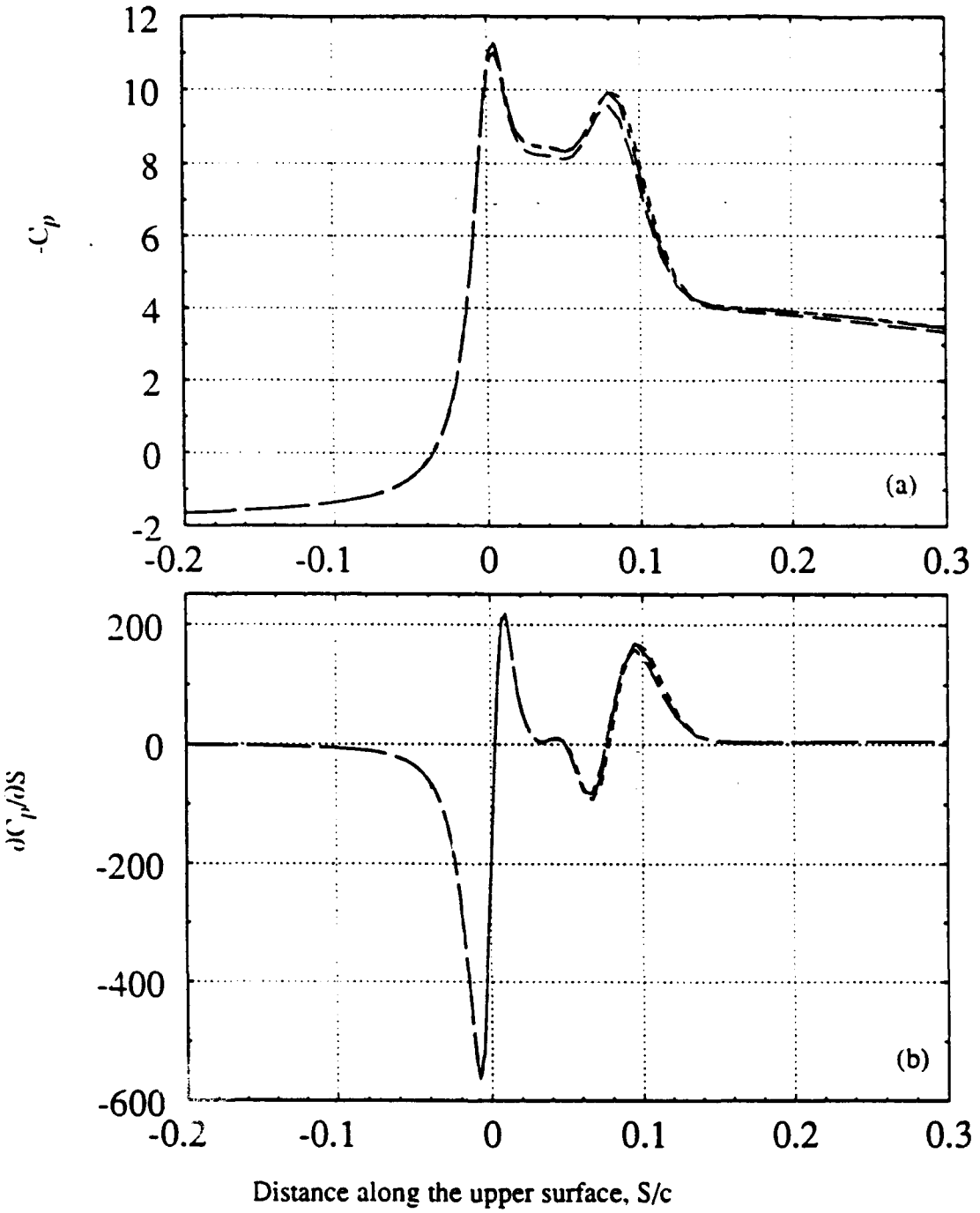

Figure 12. a) Surface pressure and b) surface pressure gradient profiles just after the onset of leading edge separation (30^0), $\Omega^* = 0.4$. ..... e = 0.039, —·— e = 0.15, and - - - - e = 0.60.

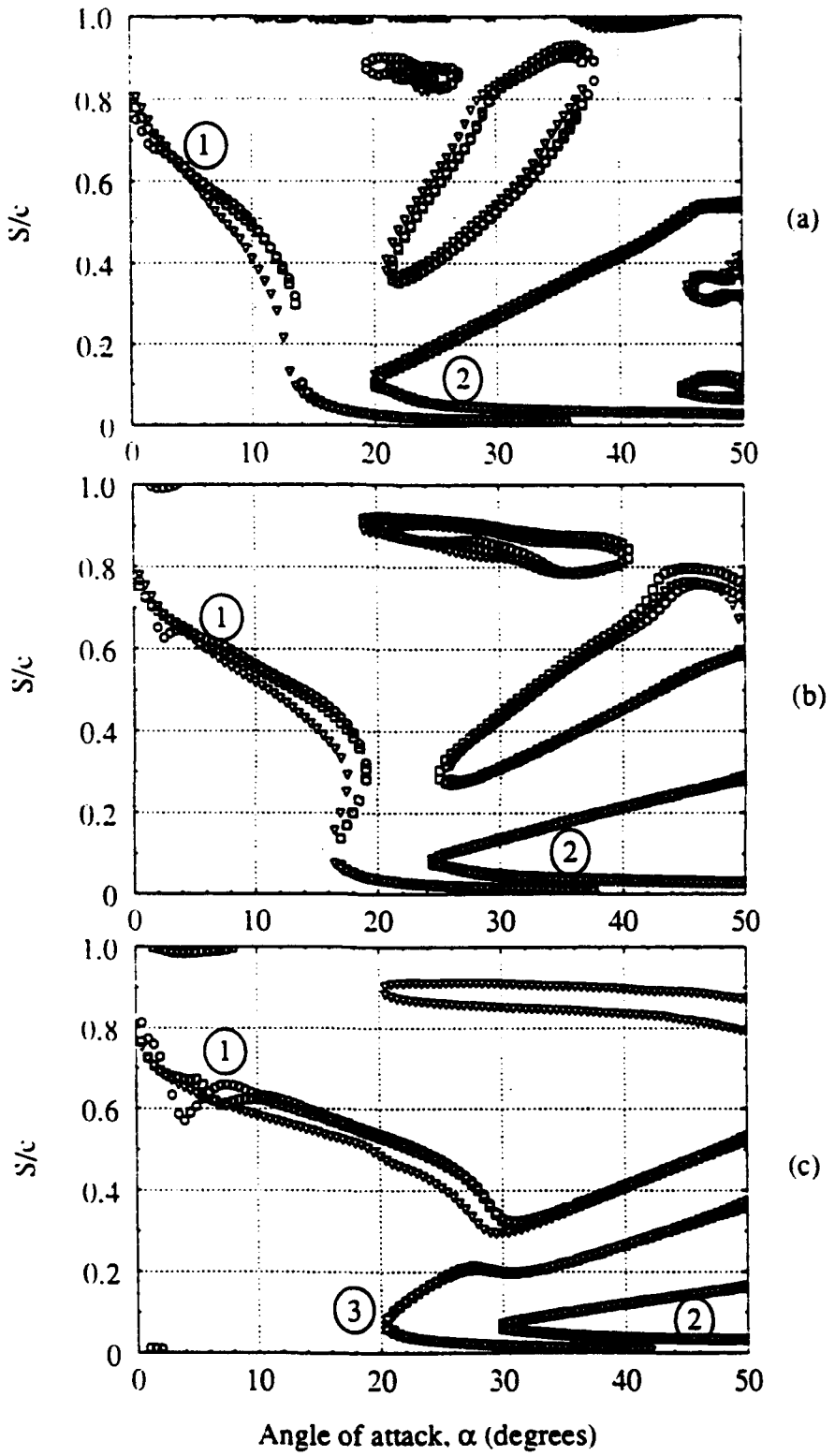

Figure 13. Tangential velocity flow reversal locations just above the airfoil surface: a) $\Omega^* = 0.1$; b) $\Omega^* = 0.2$; and c) $\Omega^* = 0.4$. ○ $e = 0.039$, □ $e = 0.15$, and ▽ $e = 0.60$. See text for a description of the curves marked 1, 2, and 3.